Spatial variability in airborne surface flux measurements during HABEX-Sahel

Frédérique Saïd, Jean-Luc Attié, Bruno Bénech, Aimé Druilhet, P. Durand, M.H. Marciniak, Bruno Monteny

Spatial variability in airborne surface flux measurements during HAPEX-Sahel

F. Saïd[a,*], J.L. Attié[a], B. Bénech[a], A. Druilhet[a], P. Durand[a], M.H. Marciniak[a], B. Monteny[b]

[a]*Laboratoire d'Aérologie, URA CNRS 354, O.M.P., 14, av. Edouard Belin, 31400 Toulouse, France*
[b]*Laboratoire d'Hydrologie, 911 av. Agropolis, BP 5045, 34032 Montpellier Cedex, France*

The spatial variability of sensible and latent heat flux measured by aircraft over a 90-km × 75-km area, near the Central Supersites of HAPEX-Sahel (Hydrologic and Atmospheric Pilot Experiment, Sahel) is discussed. The data from six flights are presented four of which were obtained during the rainy season; the others being obtained at the beginning of the dry season.

A basic difference in the behaviour of the latent heat transfer is revealed when the measurements under dry and wet conditions are compared: the latent heat flux is far more heterogeneous under drying conditions so that the estimation accuracy is reduced if the same integration length is used. It was found that under dry conditions the contribution of low frequency eddies is more important than that of local turbulence: the surface moisture is probably less homogeneous than in the wet period, but it is mostly the interaction between the marine and continental air masses linked to the closeness of the inter-tropical convergence zone that seems to drive the transfers.

Two-dimensional fields of fluxes are constructed to study their spatial variability according to the hydrological conditions. These fields are systematically compared with those of the mean parameters likely to drive the transfers. Some characteristics, common to several fields, are revealed that can be considered specific to the climate in this region, at this time of year: an east–west gradient of albedo, a south–north gradient of the sensible heat flux, surface temperature and air temperature and a north–south gradient of specific humidity. However, the aerodynamic formula that relates flux to mean parameters, fails at a 25-km × 25-km scale but gives good results at a larger scale (90 km × 75 km): at this scale, the Dalton number is around 2.5×10^{-3}.

* Corresponding author.

1. Introduction

The study of the spatial variability in surface flux is of particular relevance at the present time from the perspective of improving the surface parameterization in mesoscale and general circulation models. While there is some disagreement about the respective contribution of the different surface parameters to the evolution of weather and climate, modellers recognize the need for accurate representation of these boundary conditions (Mahrt, 1987; Segal et al., 1988, 1989; Schmugge and André, 1991; Sellers et al., 1992). The long-term objective is to enable the surface models to be calibrated directly by remote sensing, employing a limited number of in-situ measurements. However, remote sensing does not allow direct access to terms like turbulent surface flux, but merely to the parameters which govern such a flux. This is why it is necessary to examine the nature and contribution of the parameters driving surface transfer in differing climatic conditions. For example, to show how flux distribution is organized, what the sources of heterogeneity are and, given spatial variability, how an estimation of flux can be obtained from the driving parameters, especially at a scale compatible with the mesh of a mesoscale model.

HAPEX-Sahel (Hydrologic and Atmospheric Pilot Experiment, Sahel) was an intensive experimental programme with the objective of solving these problems in a region representative of the Sahelian zone and climate. The experiment is described in detail by Goutorbe et al. (1994) and Prince et al. (1995). The main objectives of the programme were (1) to study the transfer of mass and energy and, in particular, all the components of the water budget, (2) to test the performance of meteorological satellites with regard to the estimation of parameters describing the surface, atmosphere and precipitation processes and (3) to provide mesoscale or general circulation models with parameterizations which could be used to represent area-averaged flux at a scale of one grid square.

Amongst the numerous means of experimentation employed (meteorological and micrometeorological stations, balloons, aircraft and satellites), aircraft, instrumented for atmospheric measurements, played a particularly important role in the study of spatial variability in surface sensible and latent heat flux. Aircraft are a particularly effective measurement platform for describing various spatial scales. They are, however, limited in terms of the range of scales that can be resolved: the minimum sample length must allow integration of enough turbulent 'events' such that the calculation is statistically representative, and the maximum must avoid integration of low frequency variations which are no longer in the turbulence domain.

Furthermore, the minimum sample length can vary according to atmospheric conditions. In this paper, our primary objective is to calculate this minimum length of integration, under differing experimental conditions and according to the accuracy that is required for flux calculation. The result is particularly relevant to modelling. The aim is to address the following questions:

- At what minimum spatial scale (for the aircraft) can aircraft flux be compared with locally determined flux?
- At what spatial scale should surface or atmospheric parameters which control flux (direct application for remote sensing) be estimated?

Table 1

Mean characteristics of the six flights. 'z' indicates a measurement at the flight level and '10', at 10 m. The values in the table correspond to the average ± standard deviation for each flight. Symbols are defined in Section 2.3. The two different figures for Z_i (boundary layer height) account for the change of latitude as well as the thickening of the boundary layer linked to the increase of mixing

Flight number	Day	Start UTC end UTC	Mean flight level (m)	Z_i (m)	T_{10} (°C)	Q_z (g kg^{-1})	U_{10} (m s^{-1})	DD_z (°)	T_b (°C)	Z/Lmo
35	1/9/92 (245)	10:23 12:48	54 ± 13	960 1050	28.7 ± 0.6	15.4 ± 0.3	4.4 ± 1.1	243 ± 16	35.2 ± 1	− 0.7 ± 0.3
37	4/9/92 (248)	10:04 12:26	50 ± 4	600 1200	29.3 ± 0.8	16.1 ± 0.4	3.8 ± 1.1	225 ± 10	35.4 ± 1.4	− 1.4 ± 0.9
41	10/9/92 (254)	10:23 12:45	53 ± 4	540 1050	31.0 ± 0.9	15.8 ± 0.3	3.9 ± 0.7	240 ± 17	38.4 ± 0.6	− 3.1 ± 3.9
42	12/9/92 (256)	10:42 13:08	56 ± 4	550 990	29.3 ± 1.4	13.9 ± 0.7	3.8 ± 1	275 ± 8	37.2 ± 1.9	− 4.8 ± 9.6
47	25/9/92 (269)	11:15 12:16	56 ± 11	1050	33.7 ± 0.8	13.8 ± 0.8	2.1 ± 1	272 ± 18	40.9 ± 0.6	− 2.4 ± 1.6
53	3/10/92 (277)	09:56 11:47	57 ± 15	850 2100	32.5 ± 0.8	12.4 ± 0.8	3.2 ± 0.6	238 ± 15	43.6 ± 2.1	− 3.6 ± 2.7

Flight number	S_i (W m^{-2})	S_o (W m^{-2})	a	L_i (W m^{-2})	L_o (W m^{-2})	F_n (W m^{-2})	H (W m^{-2})	LE (W m^{-2})	$H + LE$ (W m^{-2})	$LE/(H + LE)$
35	898 ± 66	219 ± 20	0.24	419 ± 3	516 ± 7	582 ± 46	79 ± 14	210 ± 32	289 ± 31	0.72
37	731 ± 157	180 ± 35	0.25	432 ± 5	517 ± 9	466 ± 112	56 ± 20	144 ± 43	200 ± 54	0.72
41	958 ± 56	241 ± 17	0.25	419 ± 4	537 ± 5	599 ± 39	80 ± 18	167 ± 34	246 ± 41	0.67
42	881 ± 77	219 ± 8	0.25	414 ± 5	529 ± 13	547 ± 57	84 ± 27	170 ± 52	254 ± 46	0.66
47	964 ± 6	242 ± 9	0.25	431 ± 4	554 ± 4	598 ± 9	95 ± 20	151 ± 49	246 ± 42	0.59
53	914 ± 42	230 ± 18	0.25	419 ± 8	571 ± 15	532 ± 19	127 ± 25	118 ± 34	246 ± 44	0.47

- What is the basic scale necessary for validation of a mesoscale model covering the entire zone under study (some 200 × 200 km^2)?

We will present here six situations, of differing climatic conditions ranging from the later part of the rainy season to the early dry season. For these six situations, we will study the spatial distribution of sensible and latent heat flux, and also of those mean parameters, which can be measured from the aircraft and are likely to drive the fluxes. In a second step, we will try to point out some characteristics common to the various parameters to understand the mechanisms controlling the spatial variation of fluxes.

2. Experimental conditions

2.1. Flight plan

The results presented here are derived from measurements carried out by the Météo France Merlin IV aircraft. The days under study and the corresponding flight numbers are presented in Table 1. The measurement zone and flight plan are identical for the 6 days (Fig. 1). The aircraft flew two overlapping rectangles, at constant altitude and in a zone located in the northern part, and also to the north, of the 1° × 1° HAPEX square. The measurement altitude was around 50 m above mean relief, i.e. within the first 10% of the boundary layer thickness Z_i (which ranged, around midday, from 600 m to 2300 m throughout the period studied here; see Table 1). Under these conditions, fluxes calculated at 50 m are not significantly different from surface fluxes.

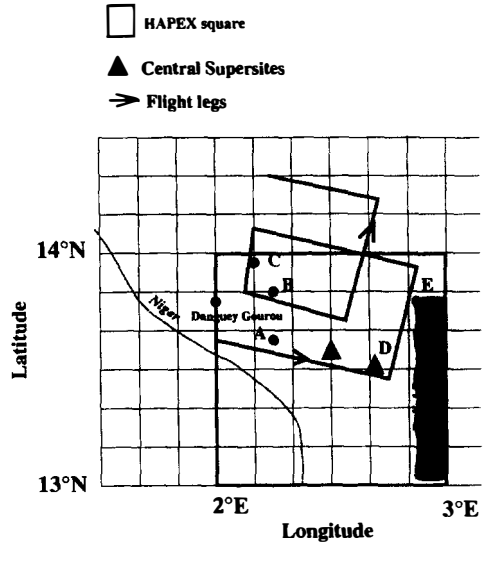

Fig. 1. Map of the flights. Also shown are the HAPEX degree square, the location of the two Central Supersites and of the Danguey Gourou site, the River Niger and west border of the Dallol Bosso and the location of the EPSAT raingauges referred to as A, B, C, D and E in Fig. 2.

At times, two other flight patterns were used: vertical soundings to determine the boundary layer height, or three superimposed legs in a vertical plane with the upper one situated at level 0.9 Z_i, to estimate the entrainment flux at the boundary layer top. One or two vertical soundings were achieved during each flight and the vertical pattern was performed along one leg only during Flights 35, 37, 41 and 42.

The aircraft were flown between 10 h and 13 h (Universal Time Coordinated, UTC), when the turbulent flux varies very little with time. Having taken this precaution, no correction was made for diurnal variation. In fact this could not have been done for the following reasons: one method of taking into account the diurnal variation is to model the diurnal variation of fluxes from ground measurements at various sites along the overflown area and to apply the results to the airborne measurements. However this method requires that the meteorological conditions are cloudless: unfortunately, the sky was cloudy most of the time so this method was not applied. Another method was used by Desjardins et al. (1992) during FIFE (First International Satellite Land Surface Climatology Project Field Experiment): it consisted in sampling the flight legs twice, in opposite directions, in a sequence that assured that all grid lines were sampled at the same mean time. While this technique is very useful, it is achieved at the expense of a considerable lengthening of the flight duration. This had to be avoided due to the already long length of the flight legs.

2.2. Variables measured

The variables measured by the Merlin IV aircraft are briefly described as follows. Static and dynamic pressure as well as angles of attack and sideslip were measured at the radome on the nose of the aircraft, as described by Brown et al. (1983). An inertial navigation system (SAGEM Ulis 45i), located near the radome, enabled measurement of the horizontal geographical coordinates of the aeroplane, its ground speed and the attitude angles of the aeroplane (roll, pitch and heading) to calculate the horizontal and vertical components of the wind velocity. A Rosemount 102E2-AL probe, a dew-point hygrometer (General Eastern) and an AIR Lymanα hygrometer measured the temperature and water vapour content, and their fluctuations.

Radiation measurements included Eppley radiometers for incoming and outgoing radiation (solid angle: 2π) in the shortwave (0.2–2.8 μm) and longwave (4–40 μm). A Barnes PRT5 infrared thermometer (8–14 μm) measured surface radiative temperature. The spatial variation of the surface emissivity, ϵ was not known. So ϵ has been taken as 1, i.e. assuming that the Barnes surface radiative temperature is the surface thermodynamic temperature. The measurement sample rate varied with respect to the response time of the instrument concerned. However, all the turbulence data was processed at 25 Hz. The latter was high-pass filtered at a cut-off frequency of 0.024 Hz (about 4 km) designed to capture at least 90% of the turbulent flux according a spectral study of the sensible and latent heat flux estimated at 50 or 60 m (see Section 3.1).

2.3. Calculations

Following Hildebrand (1991), it has been assumed that those errors linked to the

sensors' accuracy which are dependent on the calibration procedures and sampling rate of the various sensors, can be held to 5–10%.

The eddy correlation method used to calculate flux requires calculation of the fluctuations of variables acquired at high frequency. The fluctuations of a parameter are defined relative to the mean value calculated on a horizontal flight leg, of around 25 km. This sample length of 25 km is chosen as a compromise which integrates a sufficient number of turbulent events whilst avoiding low frequency variations which do not transfer flux. The relevance of this averaging length as well as the error it produces in estimated flux will be discussed in Section 3.1. Here a brief theoretical review is presented with some empirical relationships obtained by Lenschow and Stankov (1986), Lenschow et al. (1994) and Mann and Lenschow (1994) from aircraft eddy correlation measurements in convective boundary layers.

For a given averaging time (or averaging length) there is a systematic difference between the true flux or variance and the ensemble average of the time means of the same quantities. The difference is referred to by Lenschow et al. (1994) as the systematic error. It is a decreasing function of the averaging time. The variance of the time mean of the flux or variance represents the random scatter of individual measurements which is also a decreasing function of the averaging time.

2.3.1. Systematic errors

According to Lenschow et al. (1994), the systematic error in a vertical flux F is given by

$$F - \langle F(L) \rangle \simeq \frac{2F\ell_{ws}}{L} \tag{1}$$

provided $L \gg \ell_{ws}$. The brackets $\langle\rangle$ denote ensemble average. L is the averaging length of flux F, ℓ_{ws} is a Eulerian integral length scale which, in principle, can be determined from the cospectrum $C_{ws}(k)$ of w and scalar s in the limit as the wavenumber $k \rightarrow 0$:

$$\ell_{ws} = \frac{\pi C_{ws}(0)}{F} \tag{2}$$

Similarly, the integral length scales for w and s are defined from the power spectra S_w and S_s of w and s:

$$\ell_w = \frac{\pi S_w(0)}{\sigma_w^2} \tag{3}$$

$$\ell_s = \frac{\pi S_s(0)}{\sigma_s^2} \tag{4}$$

where σ_w^2 and σ_s^2 are the integrals of the respective spectra from minus infinity to infinity. Lenschow and Stankov (1986) discuss the difficulties in the experimental determination of ℓ_{ws} which in some cases becomes negative. They therefore derive an inequality giving an upper bound to the systematic error in terms of the integral scale of the scalar fluctuations ℓ_s and of the correlation coefficient $r_{ws} = \overline{w's'}(\sigma_w\sigma_s)^{-1}$:

$$\epsilon_f = \frac{F - \langle F(L) \rangle}{F} \leq \frac{2}{r_{ws}} \frac{(\ell_w \ell_s)^{1/2}}{L} \tag{5}$$

Mann and Lenschow (1994) tried to take into account the difference in the integral length scale generated by a scalar flux at the surface, compared with that resulting from a scalar flux at the top of the boundary layer. Using the results of large-eddy numerical simulations from Moeng and Wyngaard (1989), they predicted that the integral scales should be larger for scalars with significant entrainment fluxes at the top of the boundary layer – but could not prove it for lack of experimental results.

Mann and Lenschow (1994) derived from Eq. (1) another expression to estimate the systematic error contributed by the difference between using a detrended time series and a high-pass filtered time series:

$$\frac{\langle F(L)\rangle - \langle F(L_c)\rangle}{F} = bZ_i \left(\frac{Z}{Z_i}\right)^{1/2} \left(\frac{1}{L_c} - \frac{1}{L}\right) \tag{6}$$

where L_c is the cut-off wavelength of the high-pass filter. The coefficient $b = 1.2$ results from assumptions derived from empirical results which need not be described here.

The application of Eqs. (1)–(6) to the present study will be presented in Section 3.1.

2.3.2. Random errors

The calculation of the random error has been addressed by several authors from a theoretical point of view (Lumley and Panofsky, 1964; Wyngaard, 1973, 1983). Lenschow and Stankov (1986) applied the results to airborne measurement in the boundary layer. According to Wyngaard (1982), if one makes the hypothesis that the distribution of turbulent fluctuations is Gaussian, the relative accuracy of estimation of a vertical flux (calculated from the covariance of w and s) is as follows:

$$\epsilon_{ws} = \frac{\sigma_F(L)}{|F|} = \left\{ 2\frac{l_{ws}}{L}(1 + r_{ws}^{-2}) \right\}^{1/2} \tag{7}$$

$\sigma_F(L)$ is the absolute error of the vertical flux F, l_{ws}, the integral length scale of the covariance between the vertical velocity and the scalar s. It is defined as the integral of the autocorrelation function up to the first zero crossing (Lenschow and Stankov, 1986). The integral time scale obtained is converted into a length scale, using the mean true airspeed of the aircraft.

Lenschow and Stankov (1986) used experimental data obtained in convective boundary layers to derive an empirical expression for the integral scale:

$$l_{ws} = 0.16 Z_i \left(\frac{Z}{Z_i}\right)^{1/3} \tag{8}$$

where Z is the measurement level and Z_i, the boundary layer thickness. Using Eq. (8) and $r_{ws} = 0.56$, Eq. (7) becomes (Lenschow et al., 1994):

$$\frac{\sigma_F(L)}{|F|} = 1.16 \left(\frac{Z}{Z_i}\right)^{1/6} \left(\frac{Z_i}{L}\right)^{1/2} \tag{9}$$

$r_{ws} = 0.56$ is derived from the local free convection relationships for σ_w and σ_t obtained by Wyngaard et al. (1971) in the surface layer. As an example, if $Z_i = 1000$ m, $L = 25$ km and $Z = 55$ m, the relative accuracy that one can expect for heat flux at the surface is 14%.

Mann and Lenschow (1994) further improved the practical Eq. (9) by assuming a linear vertical variation of fluxes. If the flux at level Z is $F_z = (1 - a(Z/Z_i))F_o$, where F_o is the surface flux, they found that $a = 1.38$ gave the best fit to the dataset they used. They also used the results of the large eddy simulations from Moeng and Wyngaard (1989) and mixed layer empirical results obtained by Lenschow et al. (1980) to predict a sophisticated relationship for r_{ws} (Eq. (23) and Fig. 3 in Mann and Lenschow, 1994) and $(\sigma_F(L)/|F|)$ (Fig. 3 in Mann and Lenschow, 1994), depending on the entrainment ratio: $\gamma = (F_{Z_i}/F_o)$.

The specific results of our study are presented in Section 3.1.

Another way of regarding Eq. (7) is to fix the degree of accuracy that one wants to obtain and to then calculate the minimum length of integration for the flux in question. In this way the minimum spatial scale for comparison with 'local' flux can be provided.

2.3.3. Other calculations

The calculations shown in the following are mainly concerned with sensible and latent heat flux; therefore the fluctuations used apply to the potential temperature t', specific humidity q' and to the vertical velocity w'. The horizontal components of wind will also be used to calculate the friction velocity u_* and the Monin–Obukhov length, using:

$$Lmo = \frac{-u_*^3}{k\frac{g}{T_m}(\overline{w't'} + 0.61T_m\overline{w'q'})} \tag{10}$$

where $k = 0.4$, g is the acceleration due to gravity and T_m the mean temperature of the air mass.

The mean data used in this study are defined for a flight sequence of 25 km. This consists essentially of T, the potential temperature and Q, the humidity, U, the horizontal wind speed and DD its direction, as well as radiative parameters: T_b, the surface radiative temperature, S_i and S_o the incoming and outgoing shortwave radiation fluxes, respectively, L_i and L_o, the corresponding longwave radiation fluxes, F_n, the net radiation flux which is the sum of longwave and shortwave terms and a, the albedo which is the ratio of S_o to S_i.

The 'z' subscript used for mean parameters denotes that they are measured at flight level and the '10' subscript that they are measured at z, but reduced to 10 m altitude. Q cannot be calculated at 10 m since the aircraft cannot measure the surface moisture. The U and T reduction from $Z \simeq 50$ m to $Z = 10$ m was done using Monin–Obukhov theory in the surface layer ($Z \leq 0.1Z_i$). It is also assumed that the aircraft flew higher than the 'blending height' level which is considered as the minimum level from where the air is in equilibrium with a heterogeneous surface (Mason, 1988). Stability corrections for convective conditions are applied according to Dyer and Hicks (1970).

2.4. Experimental environment

2.4.1. Area description

The HAPEX-Sahel area is described by d'Herbès and Valentin (1997). The landscape is generally flat and sand-covered, with some laterite plateaux located between 30 m and 60 m above the mean ground level. Plateaux form about 25–30% of the region. The common vegetation on the plateaux is called tiger bush on account

on its striped pattern which consists in dense bands of vegetation (a few tens of metres across and a few hundreds of metres in length) separated by bare crusted soil. The plateaux edges can be steep and due to the strong run-off have little vegetation. The plateaux lengthscale is roughly 2.3 km which can be considered as the largest scale of surface heterogeneity.

At the valley bottoms, or on the lower and less steep slopes of the plateaux, the surface is covered with sand, planted with millet (57%) or left fallow (22%). The proportions of respective surface covers, which has been calculated for the whole HAPEX square, may vary a little on the area overflown as the flight legs extend 50 km further to the north. The main difference should be the increasingly higher proportion of bare soil found in tiger bush as rainfall decreases along the south–north rainfall gradient.

The area is bordered by two river valleys (Fig. 1): one is the River Niger valley to the south-west and the other is the ancient river valley of Dallol Bosso, to the east. The water-table of this latter valley often comes up to the surface during the rainy season.

The evolution of vegetation over the HAPEX area during 1992 is described by Prince et al. (1995): for the period concerned in this paper the normalized difference vegetation index (NDVI) calculated from NOAA-AVHRR (Advanced Very High Resolution Radiometer) data, indicates a contrast in vegetation cover between the 'Central Supersites' (two sites selected for intensive monitoring) and the Danguey Gourou site, situated to the east of the flight area (see Fig. 1). The NDVI at the Central Supersites increased from 0.22 to 0.24 during September and dropped to around 0.22 in the early dry season. At the Danguey Gourou site, the evolution was quite similar but the values for the same period were respectively 0.15, 0.18 and 0.16. This reflects the strong variability between two sites, 90 km apart, which may be the result of the closeness of the relatively wetter Dallol Bosso valley towards the eastern border of the area.

As a conclusion to this section, we could say that the patchiness of the HAPEX-Sahel area is rather different from that of previous land-surface experiments:

- The HAPEX-MOBILHY (Hydrologic and Atmospheric Pilot Experiment and Modélisation du Bilan Hydrique) (André et al., 1988) site was a square (100 km^2) area divided into two fairly homogeneous parts: a flat forest with large clearings with maize, and a hilly zone of undulating hills with varied cultivation in small fields (cereals, orchards, vineyards, meadows). The area contains part of the basin of the Adour river and that of a coastal river. The climate is maritime and of mid-latitude type. The data analysed during that experiment enabled André et al. (1990) to conclude that there are two types of non-homogeneous land surfaces: some 'disorganized' land surfaces with horizontal length scales smaller than about 10 km and internal boundary layers that rapidly mix up and some 'organized' land surfaces with horizontal length scales greater than 10 km, which interact with the atmosphere at the mesoscale.
- The FIFE (First International Satellite Land Surface Climatology Project Field Experiment) (Sellers et al., 1988, 1992; Davis et al., 1992) experimental site was 16 km × 16 km so its variability is necessarily of smaller scale than the variability of both HAPEX experiments. The vegetative cover within the area is not entirely homogeneous. It consists of a tallgrass prairie with some parts grazed

and others burnt. There are gently rolling hills with some woody areas in the drainage bottoms. The climate is mid-continental.

- The EFEDA (European Field Experiment in Desertification-threatened Areas) (Bolle et al., 1993) study area was a rectangle which covered more than 10^4 km^2. It is a plateau bordered by mountains to the north, east and south, and centred in the headwaters of the Guadiana Basin. The climate is of Mediterranean type and is prone to desertification in spite of irrigation. The landscape is of intensive, irrigated agriculture with varied crops (cereals), but there are also drylands with vineyards, olive groves, fallow and small forests. The horizontal lengthscales of the landscape are usually greater than those in HAPEX, in the intensively cultivated areas.

The HAPEX-Sahel landscape is less complicated than the landscapes described above, due to the limited number of different surface covers (four). Its patchiness could be compared to that described by Mahrt et al. (1994) for the California Ozone Deposition Experiment (CODE) with 5- to 15-km lengthscales and irrigated or non-irrigated areas. In addition, in the HAPEX-Sahel case, a temporal heterogeneity must be taken into account, due to the erratic occurrence of rainfall over very hydrologically different surface types (Estèves, 1994), which implies different time-scales for different processes (run-off, infiltration, storage in ponds, etc.) (Estèves and Lenoir, 1994; Peugeot et al., 1994, Peugeot et al., 1997). So the spatial aspects cannot be disconnected from the temporal aspects and this must be kept in mind in the following analysis.

2.4.2. Meteorological conditions

The meteorological conditions encountered during the experiment were directly influenced by the north–south seasonal migration of the inter-tropical convergence zone (ITCZ). The ITCZ is a zone where two air masses meet, with one coming from the sea (south/south-west) and the other from the continent (east/north-east). At the beginning of September, the ITCZ at the longitude of Niamey (2°E, 13.5°N), was situated at a latitude of roughly 18°N. It moved slowly south during September, closer to Niamey (16–17°N on 23 September, 15°N on 26 September) whereas it was already at 12°N over Tchad (situated to the east of Niger) during this same period. The ITCZ moved away to the north from 28 September (16°N) to 30 September (17–18°N), but came closer to Niamey on 5 October (16°N).

Thus the ITCZ remained north of Niamey during the whole of the campaign and the flights were conducted within a warm and moist south-south-westerly monsoon flow coming from the Gulf of Guinea. The depth of moist flow varied and progressively decreased towards the end of the rainy season, in accordance with the position of the ITCZ. Above this humid layer there was warm, dry and generally dusty air coming from the Sahara Desert (to the east): the Harmattan. This capping layer was encountered within the first 1000 m by the end of the campaign (Wai et al., 1997).

2.4.3. Rainfall

Rainfall was recorded using the EPSAT-Niger (Estimation of Precipitation by SATellite, Niger experiment) raingauge network implemented by the Institut National

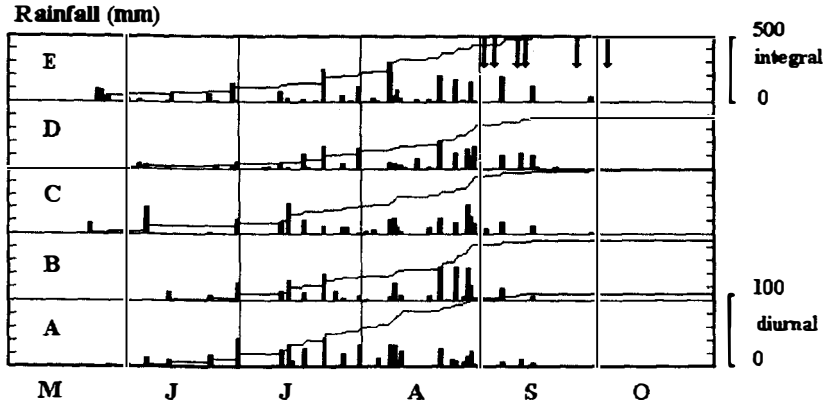

Fig. 2. Daily rainfall and cumulated seasonal rainfall measured by ORSTOM with the EPSAT raingauge network at the five stations shown in Fig. 1. Arrows indicate flight days.

de Recherche Scientifique pour le Développement en Coopération (ORSTOM) (Lebel et al., 1992). Fig. 2 shows the records of five stations situated at different places in the flight area (see Fig. 1). The dates of the flights discussed in this paper are shown on the same figure. One can see that rainfall stopped after mid-September at most stations. Thus, four of the six flights studied here were in the rainy season, and the two remaining were at the beginning of the dry season. However Fig. 2 shows that the spatial variability of rainfall is strong. For instance, the rainfall event of 11 September, just before Flight 42, only affected Stations A and D which are situated to the south of the area. The isohyets corresponding to this rainfall event are shown on Fig. 3: we can see that no rainfall was recorded to the north of latitude 13°40 N so that the area which is overflown the next day (Flight 42) should present rather heterogeneous conditions.

The antecedent rainfall conditions for flight analysed were:

Flight 35: 2 days after repeated rainfall events

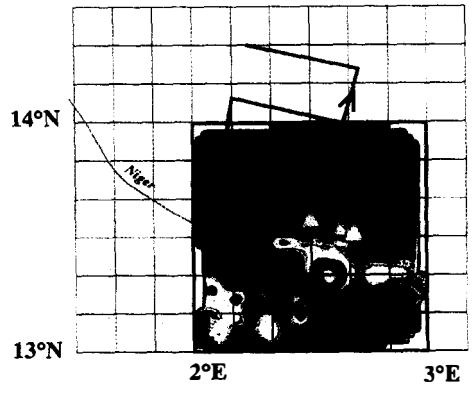

Fig. 3..Isocontours of rainfall recorded on 11 September with the ORSTOM EPSAT raingauge network. The flight lines and the location of the Central Supersites are also indicated.

Flight 37: 3 days after rain
Flight 41: 4 days after heavy rain
Flight 42: 1 day after rain
Flight 47: 10 days after last rain
Flight 53: 18 days after last rain

2.4.4. Mean radiative and thermodynamic parameters

An alternative way to see the change between the two seasons is to examine the time evolution of the daily maximal surface temperature as measured by the ORSTOM team (Fig. 4). It can be seen from this figure that the surface temperature fluctuates widely during the rainy period. The whole period reveals an increase in the surface temperature from around 35°C during the first part of September, to 45°C at the beginning of October.

Table 1 summarizes the mean meteorological conditions encountered over the six flights. The values correspond to the average (and standard deviation) of the measurements calculated for the 15 legs of each flight. The first point is that the albedo remains constant throughout the period (around 0.25), which implies that the evolution of the vegetation has no influence on surface albedo for this scale of time and space. The standard deviation of the shortwave incoming radiation indicates that there were often cloudy conditions. Flight 37 was the most cloudy day (low value of S_i: 731 W m^{-2} and high standard deviation: 157 W m^{-2}) whereas Flight 47 was clear ($S_i = 964 \pm 6$ W m^{-2}). This latter flight is also characterized by the presence of much dust, which is not immediately obvious from the radiation values, because the slight increase of L_i is of the same order of magnitude as the accuracy. Flight 53 is also slightly dusty. After the end of the rainy season there are fewer clouds so the mean incoming shortwave radiation increases slightly. On the other hand, the surface radiative temperature continues to increase by about 8°C during the course of the month. The consequence (since S_o is proportional to S_i, and since L_i is more or less constant) is that the net radiation decreases during the month from 582 to 532 W m^{-2}. On the other hand, after some variations at the beginning of September, the available

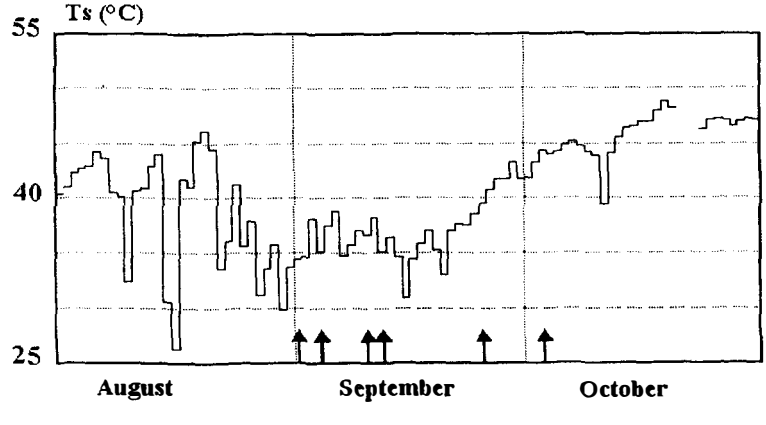

Fig. 4. Time series of the daily maximal surface temperature measured at the East Central Supersite by ORSTOM. Arrows indicate flight days.

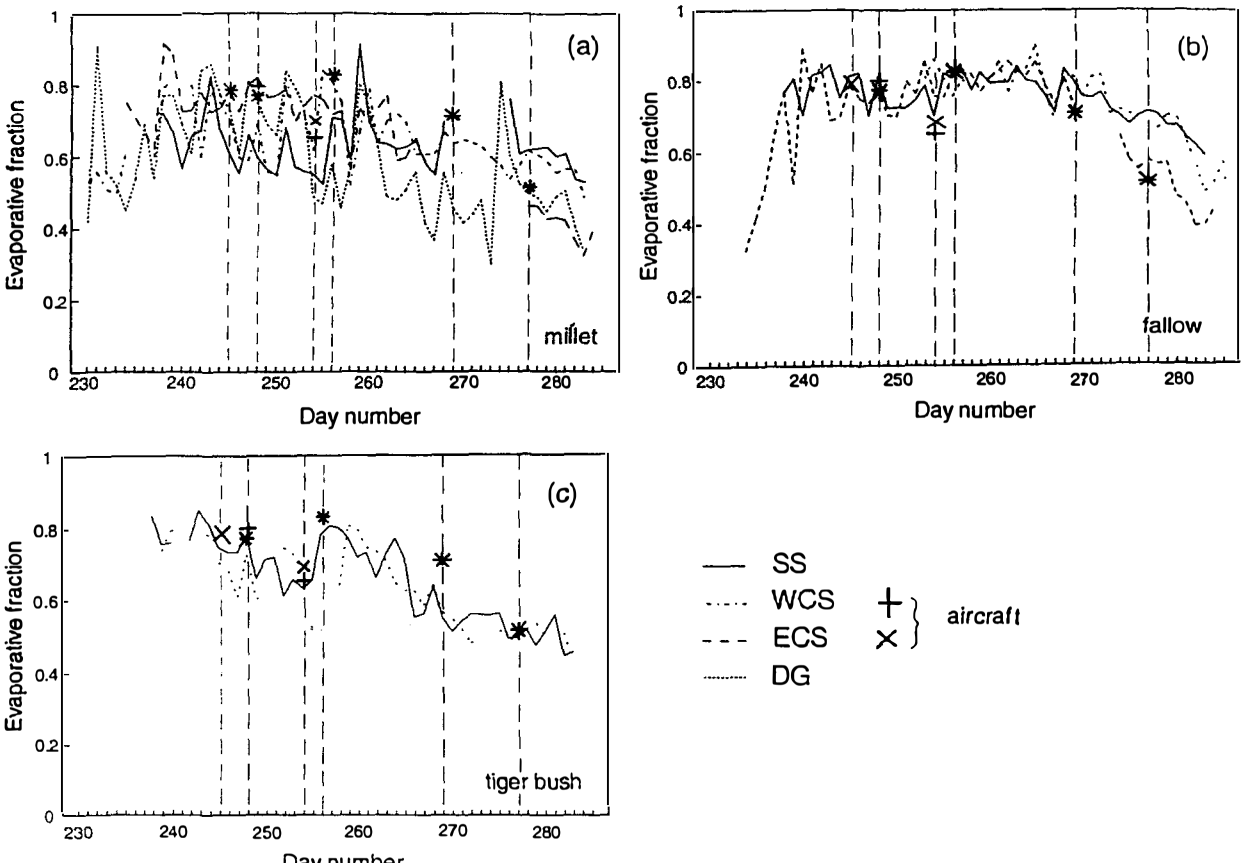

Fig. 5. The evolution of the daily evaporative fraction measured at three supersites during the IOP for (a) the millet sites, (b) the fallow sites and (c) the tiger bush sites. (Redrawn from Gash et al., 1997). The evaporative fraction measured by the Merlin IV in the vicinity of WCS (+) and ECS (×) are superimposed. (*) are used when (+) and (×) are the same.

energy $H + LE$ (sum of the sensible and latent heat flux) remains almost constant from Flight 41 to Flight 53.

The wind at 10 m is rather low during the whole period (1.4 to 4 m s^{-1}). While the surface radiative temperature increases during the period, the air mass becomes hotter and drier: the temperature (at 10 m) increases from 28.7 to 32.5°C and the humidity decreases from 15.4 to 12.4 g kg^{-1}.

2.4.5. Turbulent fluxes

The trend depicted above also appears in the turbulent fluxes: the sensible heat flux increases from 79 to 127 W m^{-2}, while the latent heat flux decreases from 210 to 118 W m^{-2}. The stability conditions remain unstable throughout the period and show a trend to an increasing instability from the wet to the dry period as can be seen from the evolution of the stability parameter *Z/Lmo* (Table 1). The strong and highly variable instability of Flights 41 and 42 is due to occasional local low values of the friction velocity, on these specific days.

In contrast to the behaviour of the fluxes, the evaporative fraction *EF* (latent heat flux divided by the available energy) decreases from 0.72 to 0.47.

Gash et al., 1997 compared the evaporative fraction values obtained by all micro-meteorologists during HAPEX-Sahel, at the various supersites and over the three kinds of surface cover: fallow, millet and tiger bush. The corresponding time series are redrawn in Fig. 5 and compared with the aircraft measurements collected in the vicinity of the West Central Supersite (WCS) and East Central Supersite (ECS). The aircraft data correspond to the flux estimation at the time when the aircraft overflew the supersites which usually happened between 10:30 and 11:30 h (UTC). The data from Gash et al. (1997) are daily values. Except for the tiger bush, which is clearly not the main surface cover overflown, there is good agreement between the aircraft estimates and the surface evaporative fraction measured at WCS and ECS. More accurately, the sharp increases after recent rainfall (Days 245, 248, 256) and the decreases in proportion as the time elapsed after the last rainfall (Days 254, 269, 277) are well correlated.

Table 2

Evaporative fraction from aircraft measurements in the vicinity of the East Central Supersite or measured by the ORSTOM team at the same supersite in a fallow and a millet site, at the flight hour

Date	Hour	Aircraft	Fallow	Millet
1/9/92	10:35	0.79	0.78	0.33
(245)	11:35	0.77	0.71	0.46
4/9/92	10:20	0.79	0.82	0.69
(248)	11:20	0.77	0.77	0.88
10/9/92	10:30	0.69	0.64	0.76
(254)	11:30	0.71	0.70	0.76
12/9/92	10:55	0.84	0.84	0.82
(256)	11:55	0.80	0.76	0.79
25/9/92	11:20	0.72	0.57	–
(269)				
3/10/92	10:10	0.52	0.50	0.55
(277)	11:30	0.50	0.48	0.38

The comparison shown in Fig. 5 follows a study by Brutsaert and Sugita (1992) who used FIFE data to check that values of $ER = LE/F_{ER}$ (F_{ER} being either F_n, G, soil heat flux, H, $F_n - G = H + LE$, or any component of the net radiation, S_o, S_i, L_o and L_i) were constant through the day. In this way total daytime evaporation fraction can be estimated with two or more estimates of instantaneous values. These conclusions were assumed to be valid in the case of the Sahelian boundary layer after consideration of the shape of the diurnal evolution of the components of the surface budget at the three supersites (Lloyd et al., 1997). The shapes of the various components are very similar at least in the morning when the fluxes are increasing and during the middle of the day. For confirmation, Table 2 shows the agreement between the instantaneous values of EF measured by the ORSTOM team at the fallow East Central Supersite and the aircraft estimate for that area. On the other hand the measurements at the millet site also quoted in the table show large discrepancies for at least 3 days.

The conclusion of this brief comparison of aircraft estimate of evaporative fractions with local measurements is that the agreement is good and is better if it is considered that the main surface cover overflown was fallow.

3. Results

3.1. Integral scales and minimum sample length

The intention in this section is to verify the suitability of the sample length of 25 km, for the boundary layers under study, and to find out if it is possible to reduce this integration length to obtain flux estimates at spatial scales closer to those of the local measurements. Alternative aims are the estimation of the error associated with the flux calculation and checking the applicability of the empirical relationships shown in Section 2.3 to the case of the boundary layers under study.

Eqs. (1) and (7) imply that estimation of the minimum length for calculating flux requires prior study of integral scales for transfers and coefficients of correlation between the variables involved. These parameters were calculated for each of the 15 25-km flight legs for each flight and for the high-pass filtered covariances $\overline{w't'}$ and $\overline{w'q'}$. The results are presented in Table 3 in the form of mean values and standard deviations for each flight.

It can be seen that the integral scales of $w't'$ and $w'q'$ are of the same size (25 to 36 m)

Table 3

Correlation coefficients (r_{wt} and r_{wq}), integral length scales (l_{wt} and l_{wq}) (m), relative accuracies for 25-km legs (ϵ_{wt} and ϵ_{wq}) and integration lengths (L_{wt} and L_{wq}) (km) for a 20% accuracy

Flight	r_{wt}	r_{wq}	l_{wt}	l_{wq}	ϵ_{wt} (%)	ϵ_{wq} (%)	L_{wt}	L_{wq}
35	0.60 ± 0.03	0.48 ± 0.05	34 ± 7	33 ± 7	10	12	6.4	8.8
37	0.59 ± 0.04	0.43 ± 0.07	25 ± 7	25 ± 8	9	11	4.8	8.0
41	0.62 ± 0.08	0.44 ± 0.07	30 ± 6	30 ± 3	9	12	5.4	9.2
42	0.60 ± 0.04	0.45 ± 0.09	36 ± 10	34 ± 8	10	13	6.8	10.1
47	0.61 ± 0.02	0.27 ± 0.08	33 ± 6	40 ± 9	10	22	6.1	29
53	0.63 ± 0.03	0.27 ± 0.07	31 ± 5	42 ± 10	9	24	5.5	31

except in the case of latent heat in dry conditions (40 to 42 m for the flights of 25 September and 3 October). The correlation coefficient for sensible heat (0.59–0.63) is high. It is higher than the average of the coefficients (0.56) calculated by Druilhet et al. (1983) in a statistical study of diverse convective boundary layers and consistent with the coefficient (0.60) obtained by Durand (1983) during the ECLATS (Etude de la Couche Limite Tropicale Sèche) experiment in the Sahel. This coefficient is also higher than the coefficient deduced from surface layer similarity theory (0.56, see Section 2.3), but the fundamental difference is that this theory does not differentiate between r_{wt} and r_{wq}. Here, the correlation coefficient for latent heat flux varies from 0.43 to 0.48 in wet conditions, which is again rather high compared to the value of 0.40 found by Druilhet et al. (1983) and Durand (1983). However this coefficient becomes very low (0.27) in dry conditions.

Both results for integral length and correlation coefficients show that the transfer of sensible heat is not influenced by the change in hydrological conditions. On the other hand, the latent heat transfer, which behaves like the sensible heat flux in wet conditions, becomes different when the hydrological conditions change. This result is not consistent with the results presented by Lenschow and Stankov (1986) who do not note any difference between both scalars t and q when calculating the integral scales. Furthermore, if Eq. (8) is applied to the results presented here, it yields high l_{ws} values, which vary between 40 m and 101 m (according to the flight and boundary layer value that is used). This can be explained by the fact that Eq. (8) results from a fit to data obtained in the mixed layer whereas ours are from the surface layer.

From the relationship for r_{ws} calculated by Mann and Lenschow (1994) (their Eq. (23)) it is possible to differentiate between the sensible and the latent heat flux in so far as the entrainment ratio, γ, was found to differ between the two cases: it is $\simeq -0.1$ in the case of the sensible heat flux, whereas it may vary from 0.5 to 1.6 for the latent heat flux (Flights 35, 37, 41 and 42). With Z/Z_i ranging between 0.03 to 0.1, this leads to $r_{wt} \simeq 0.52$ which is a little underestimated and $r_{wq} \simeq 0.46$ which is a very good fit under wet conditions (γ is not available for the two flights in dry conditions).

Using Eq. (5) and $L = 25$ km to estimate the upper bound on the systematic error, the results are presented in Table 4 as the average of the results for wet and dry conditions. The upper bounds on the systematic errors obtained are very low. However, if we take into account the error linked to the high-pass filtering ($L_c \simeq 4$ km), Eq. (6) gives a systematic error which is increased to 6%. This means that the filtered signal gives a 6% lower flux compared with the unfiltered, which is consistent with the results presented in the following. If the integration length is reduced to 10 or 5 km, the error due to filtering will decrease, because it scales with $1/L$ (see Eq. (6)), but the systematic error given by

Table 4

Mean correlation coefficients, integral length scales for w, t and q and upper bound estimations on the systematic error

	r_{ws}	l_w (m)	l_s (m)	ϵ_f (%)
H	0.61	69	82	1
LE (wet)	0.44	69	126	2
LE (dry)	0.27	69	161	3

Eq. (1), which scales with $1/L$, will increase. The resulting error will remain low: 15% in the worst case.

The random error calculated from Eq. (7) for each flight is presented in Table 3. Given the sample length chosen (25 km), the relative accuracies $\epsilon_{ws} = \sigma_F/|F|$ are:

- sensible heat: 9 to 10% in all conditions
- latent heat: 11 to 13% and 22 to 24% in wet and dry conditions, respectively

If these results are compared with the empirical relationships from other experiments, the errors due to the overestimation of l_{ws} in Eq. (8) would be expected to be greater. Previously Eq. (9) yielded $\epsilon_{ws} = 14\%$, which is too high for either sensible heat or latent heat in dry conditions. The Mann and Lenschow (1994) relationships (their Fig. (3)) involving γ yield $\epsilon_{wt} \simeq 14\%$ and $\epsilon_{wq} \simeq 18\%$, which is also an overestimation for the dry period. In a study on boundary-layer moisture regimes based on data collected during the HAPEX-MOBILHY and FIFE experiments, Mahrt (1991) pointed out considerable differences in the behaviour of the sensible heat and latent heat fluxes which he explained by the large boundary-layer eddies for which "temperature and moisture near the surface become negatively correlated on scales larger than a few kilometers associated with cool moist regions and warm dry regions. On the 10 km scale, such moisture variations appear to be associated with large boundary-layer eddies and downward transport of entrained warm dry air." The data presented here do not show that the entrainment transports increased from the wet period to the dry one. However, there is an alternative evidence of the contribution of large eddies during the dry period: the contribution of low frequencies to the flux has been estimated by computing the ratio $r = F_f/F_u$ (4-km high-pass filtered flux over non-filtered flux) for each 25-km flight leg. The results are presented in Fig. 6. They are arranged in two parts involving respectively Flights 35, 37, 41 (first period) and 42, 47 and 53 (second period) due to their common characteristics. Fig. 6 shows the percentage of flight legs for which r lies in the following ranges:

$$r < 80\% \quad 80\% < r < 90\% \quad 90\% < r < 100\% \quad 100\% < r < 120\% \quad r > 120\%$$

During the first period and for 70% of the flight legs, the filtered sensible heat flux accounts for more than 90% of the total flux (which is consistent with the estimation of the systematic error (6%) due to filtering). During the second period, only 48% of the flight legs remain in this range and 45% lie in the 80–90% range. As a digression, this result is consistent with the conclusion of some experimenters in FIFE (Grossman, 1992; Betts et al., 1992; Desjardins et al., 1992), who cited the high-pass filtering as a possible source of the underestimation of aircraft flux relative to the surface measurements. However, as the HAPEX-Sahel data have not yet been completely analysed it is not possible to draw such a conclusion here.

Fig. 6 shows important differences in the low frequency contributions between the two fluxes. During the first period the low frequencies in the latent heat flux ($r < 80\%$ or $r > 100\%$) account for 14% of the cases, whereas it accounts for 67% in the second period. The cases when $r > 100\%$ correspond to counter-gradient covariances at low frequency. The number of legs showing counter-gradient covariances increases as the dryness and the heterogeneity increase.

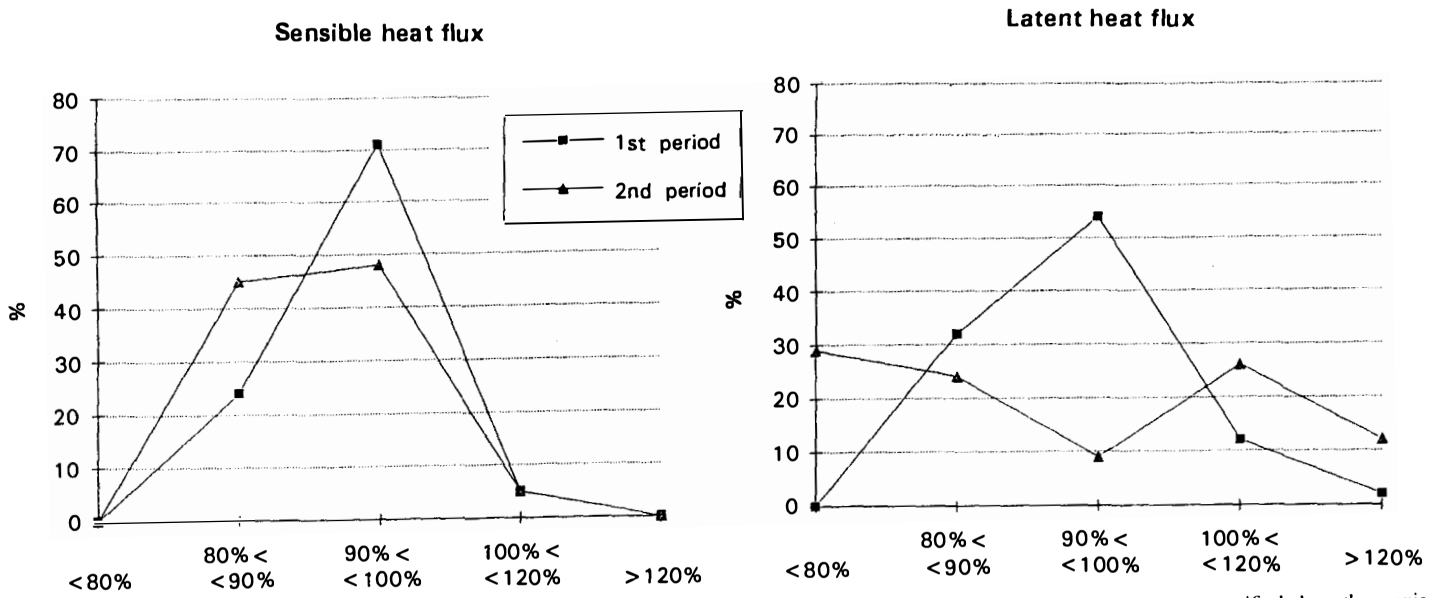

Fig. 6. Percent of legs for which the ratio of the high-pass filtered sensible heat flux (left) or latent heat flux (right) is situated in the range specified along the x axis. Flights 35, 37, 41 (1st period): squares. Flights 42, 47, 53 (2nd period): triangles.

These results tend to show that when the heterogeneity begins to appear, some low frequencies (which are excluded from the flux calculation) may interact with the latent heat fluxes by decreasing the correlation in the turbulent flux frequency range. According to Desjardins et al. (1992) and Mahrt et al. (1994), the relative variations of the high-pass filtered fluxes are more likely to be well correlated to the variations in surface properties. For this reason, some differences between the two periods should be expected, when, in the following, there is an attempt to show relationships between the turbulent fluxes and surface parameters.

As a conclusion to this subsection, we see that the calculated random errors are at least twice the systematic errors. The calculation of latent heat flux becomes much less accurate in very dry conditions. This result implies that atmospheric and surface conditions in the dry period prohibit any attempt to calculate evaporation flux at a spatial scale smaller than about 25 km. On the other hand, this should be possible for sensible heat flux in all conditions and latent heat flux in wet conditions, though with a reduction in accuracy. Thus, Table 3 shows the averaging lengths L_{wt} and L_{wq}, corresponding to an accuracy of 20%. It is clear that it would be possible to calculate sensible heat flux over legs of 5 to 7 km and latent heat flux in wet conditions, over legs of 8 to 10 km, if 20% accuracy was accepted. In this case, for spatial variability of flux to remain significant, variations would have to be more than 20%. In the following, the previous integration length of 25 km is kept to use measurements of optimal accuracy for intercomparison.

3.2. Two-dimensional fields of flux and driving parameters

In this section the turbulent fluxes of sensible heat and latent heat and the mean parameters are used to build two-dimensional fields. Around 15 legs per flight are used to build a two-dimensional field. The corresponding measurements are interpolated and smoothed. The resulting fields are 90 km from north to south and 75 km from west to east (Fig. 7). The interval between two successive contour lines as represented in the field of a variable is at least equal to the accuracy of measurement so that the spatial variation can be considered significant. The interval separating the contour lines can therefore vary with the absolute value of the variable. The colours of the fields are useful in that they show the gradient. However, they are defined with respect to field extrema and so vary, for any one variable, from one flight to the next.

The fields are described below with the principal aim of finding the differences that exist between the different conditions and, for each one, attempting to pick out the parameters responsible for the spatial variability in flux. For instance, the fields of sensible heat flux are analysed using the aerodynamic bulk formula that relates flux to mean parameters:

$$\overline{w't'} = C_t U_{10}(T_s - T_{10}) = C_t U_{10} \Delta T \tag{11}$$

where T_s is the surface thermodynamic temperature, ΔT is the temperature difference between surface and 10 m, and C_t, the aerodynamic transfer coefficient for temperature, also called Stanton number. Making the approximation that $T_s = T_b$, can lead to a maximum error of almost 1.5°C in surface temperature, if it is considered that the emissivity ϵ can vary by 2% during the flight ($\delta T_s/T_s$ = 1/4 $\delta\epsilon/\epsilon$). Given the ΔT values

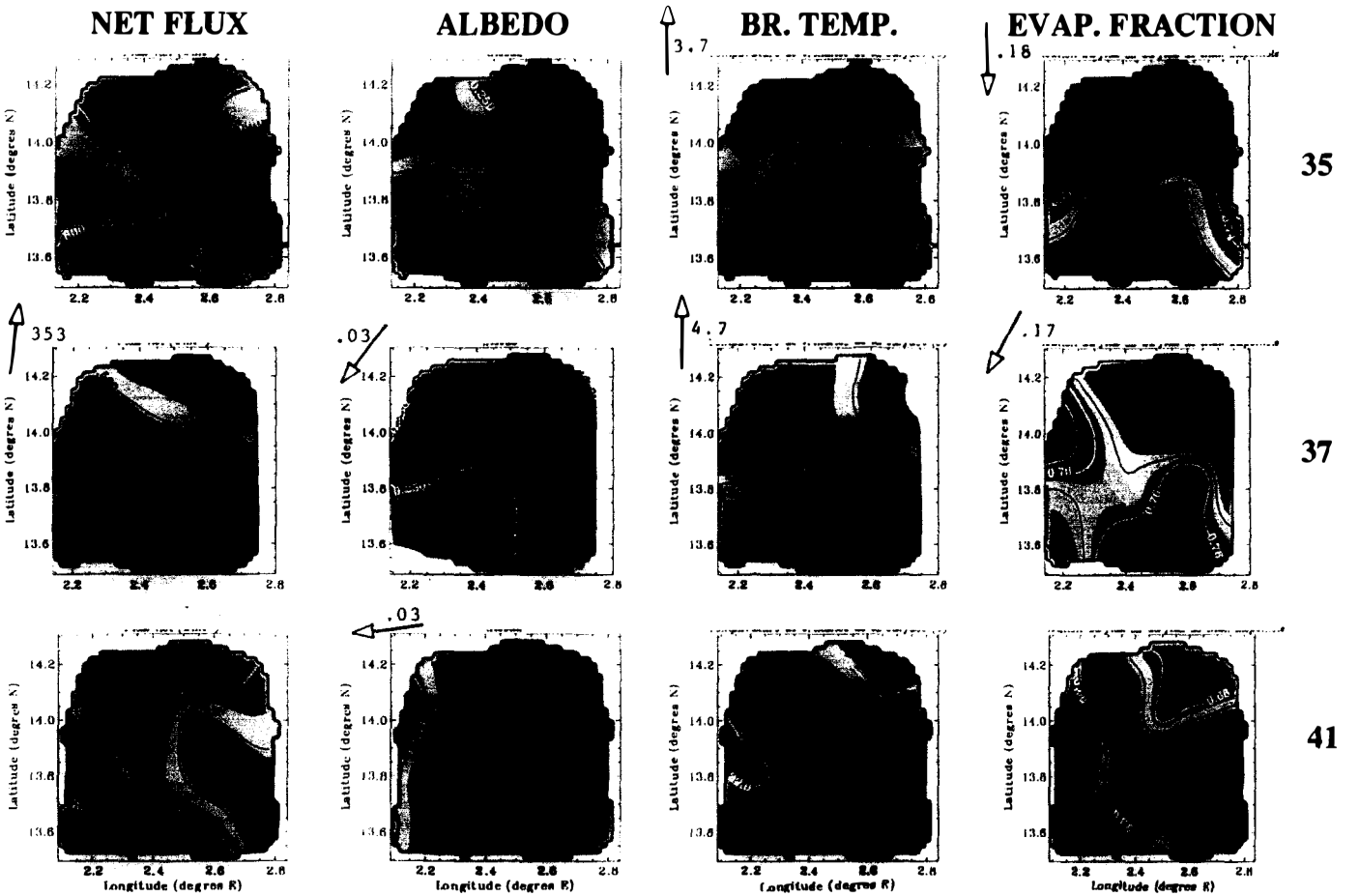

Fig 7 Isocontours of various parameters measured by the Merlin IV aircraft during the six flights: (a), (b) Net radiation flux (W m^{-2}), albedo, surface radiation temperature (°C), evaporative fraction; (c), (d) latent heat flux (W m^{-2}), humidity measured at the flight level (g kg^{-1}), horizontal windspeed reduced to 10 m (m s^{-1}); (e), (f) sensible heat flux (W m^{-2}), windspeed reduced to 10 m times temperature difference between surface and air (m °C s^{-1}), temperature difference between surface and air (°C), air temperature reduced at 10 m (°C) The arrow indicates the gradient direction, and the figure the gradient value per 100 km.

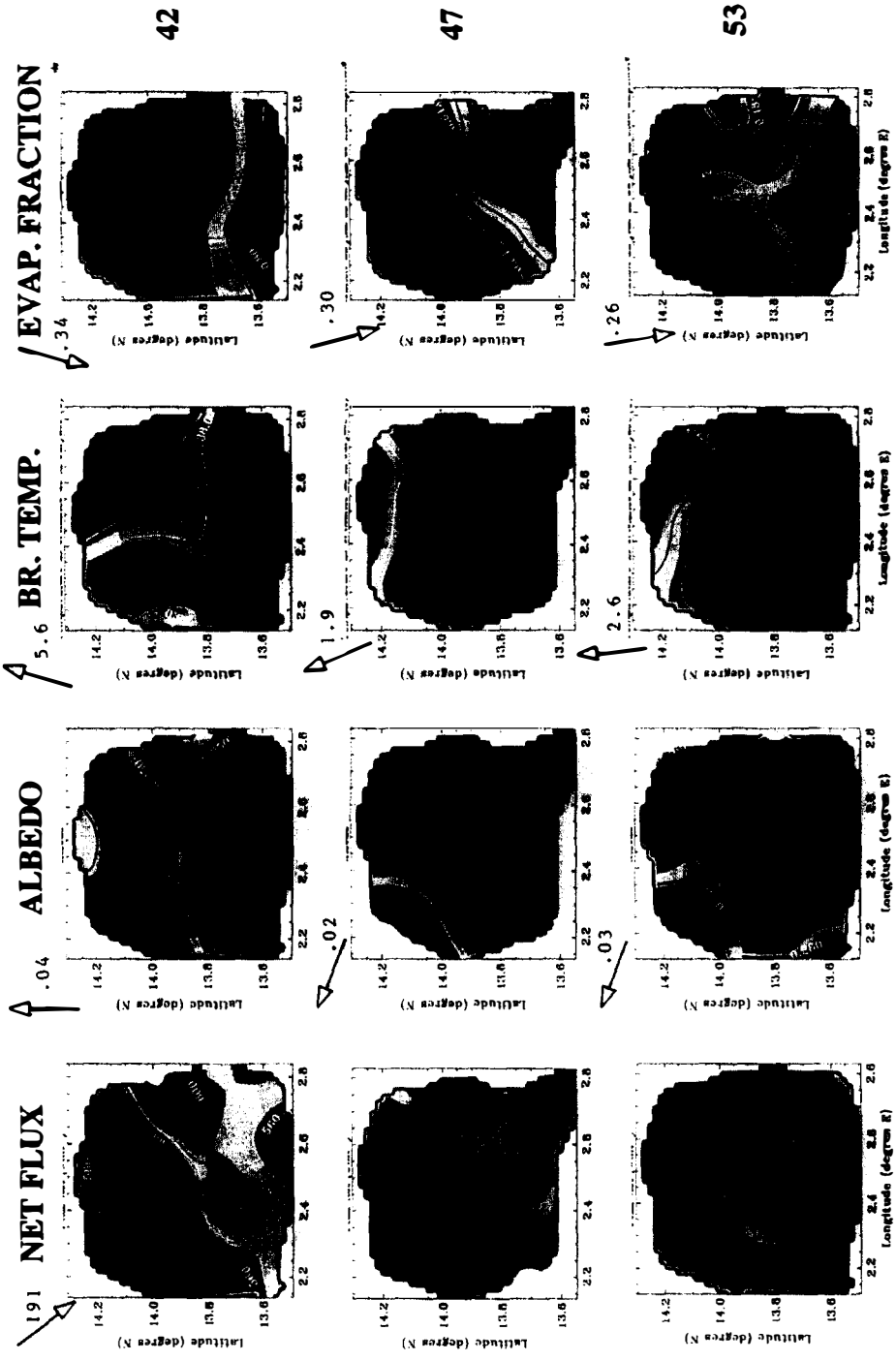

Fig. 7. Continued.

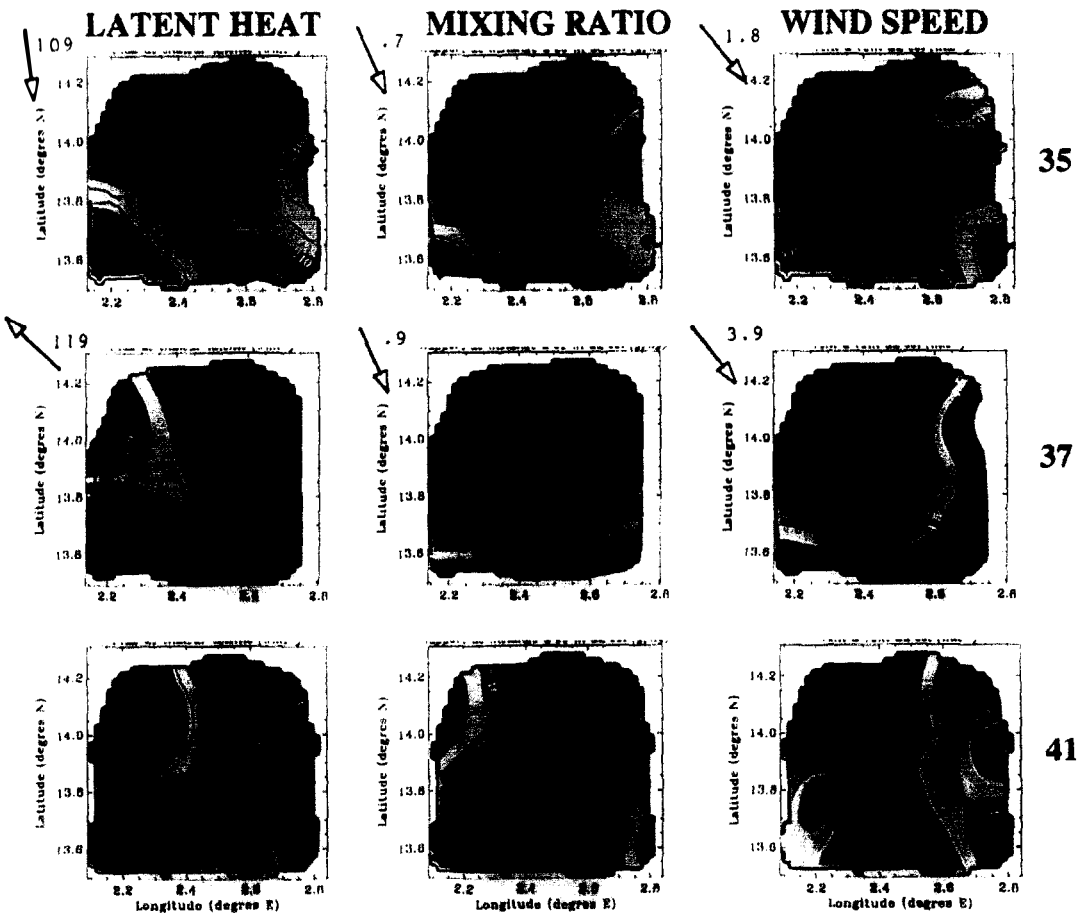

Fig. 7. Continued.

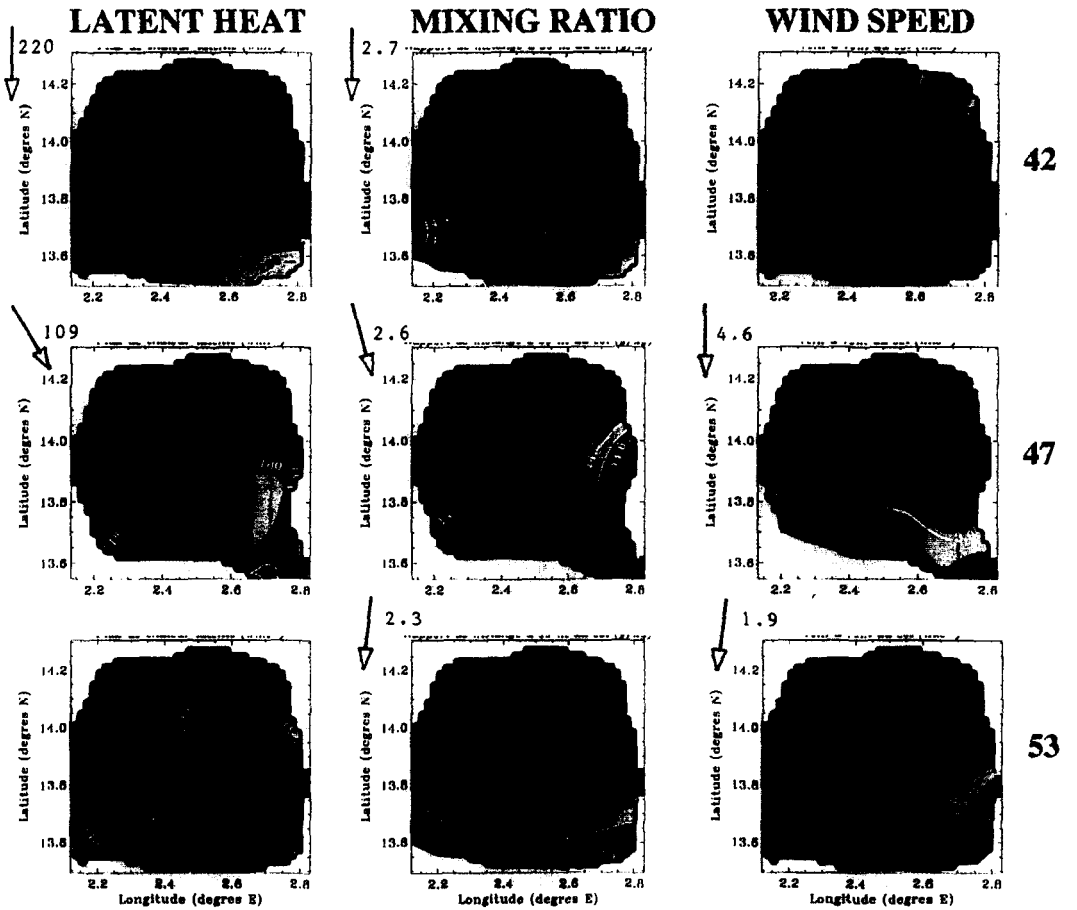

Fig. 7. Continued.

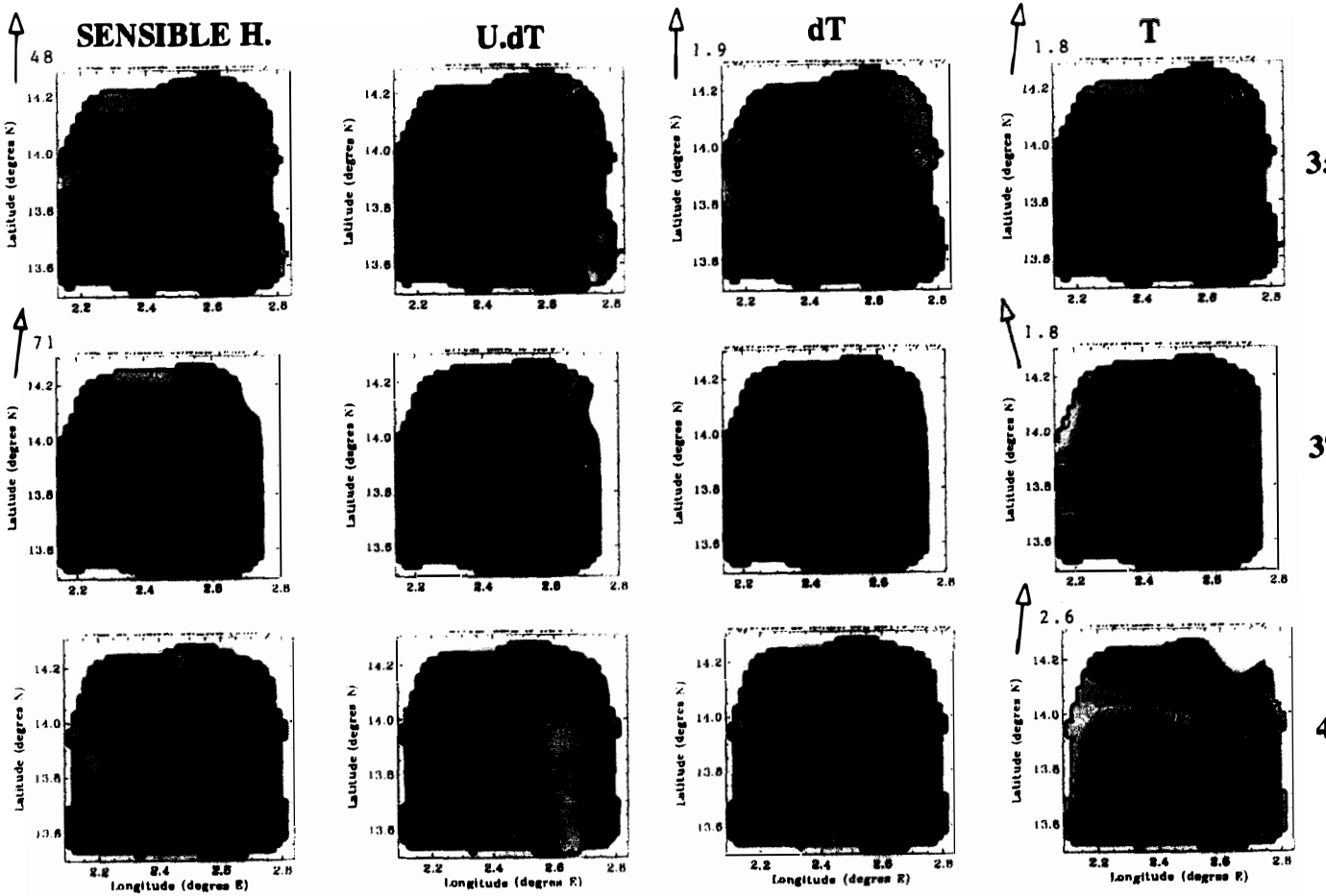

Fig. 7. Continued.

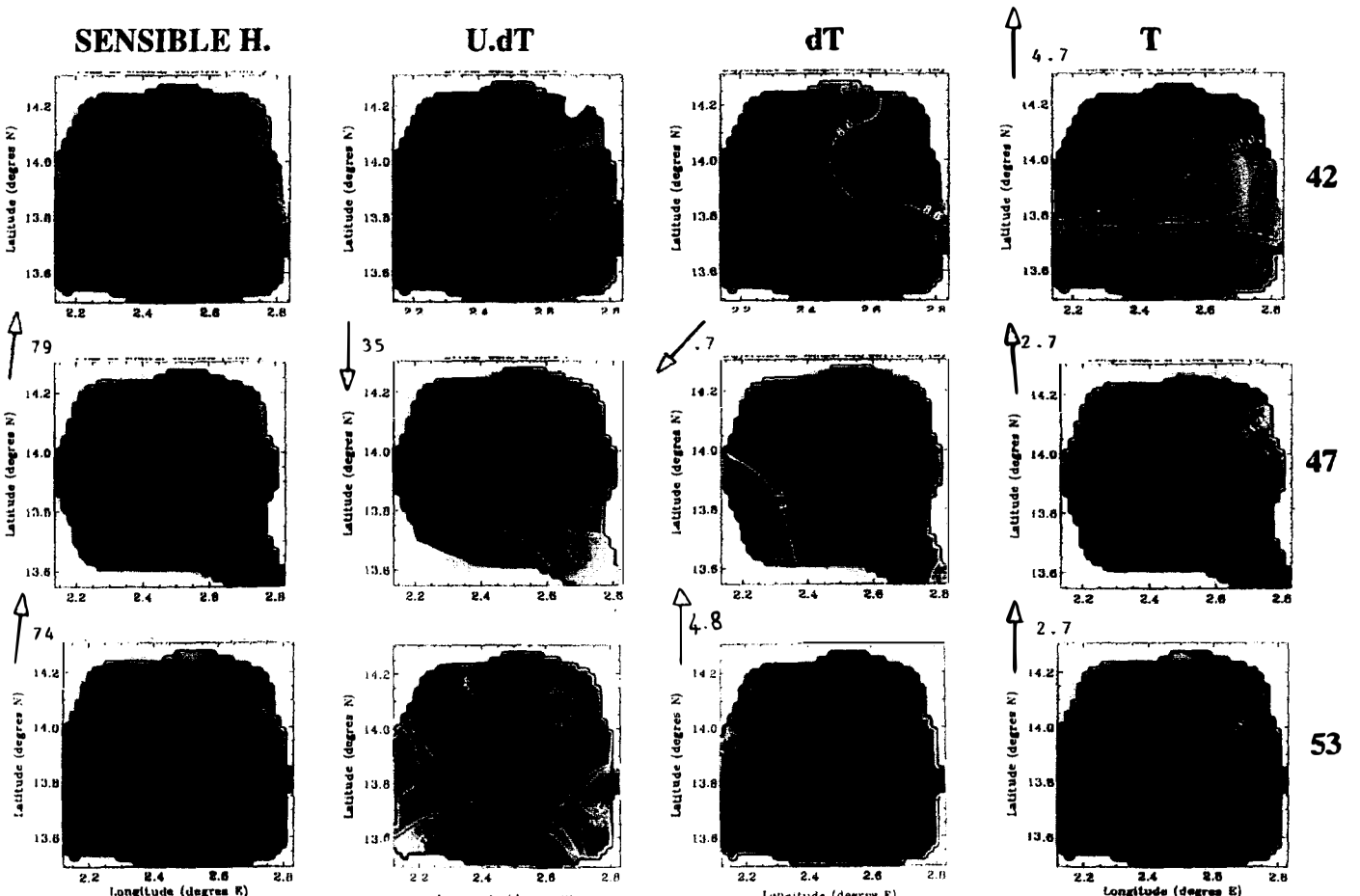

Fig. 7. Continued.

calculated for the different flights, this leads to an error of 25% on C_t. The different terms of Eq. (11) will be presented in the shape of bidimensional fields. The field of $U_{10} \cdot \Delta T$ will also be shown.

To identify characteristic horizontal variations of the various fields and to quantify the gradients, the following calculation was made: each value 'v' of the field of a variable is associated with an arrow (x, y) where x and y are the horizontal coordinates. Each arrow is projected in a given direction from which a diagram of 'v' against a distance is obtained. The direction of projection may vary between 0 and 360° and the diagram 'v' against the distance consequently varies. A horizontal gradient is detected if the correlation coefficient of the regression line fitted to these latter diagrams is the highest (among the different directions of projection) and greater than 0.7. The selected direction is the direction of the gradient and the slope of the regression line, the gradient value (expressed per 100 km). The gradient values and direction are presented in Fig. 7. The estimated gradient may be greater than the total variation in each field when the detected gradient is located in a limited area of the field.

In the following, each field will be briefly described for the various days and variables, and the temporal variation of each parameter will then be analysed with special attention focused on reproducible characteristics. In order to summarize the spatial variations of the two-dimensional fields, Fig. 8 shows the time evolution of the average per field for each parameter as well as the extreme values for each field.

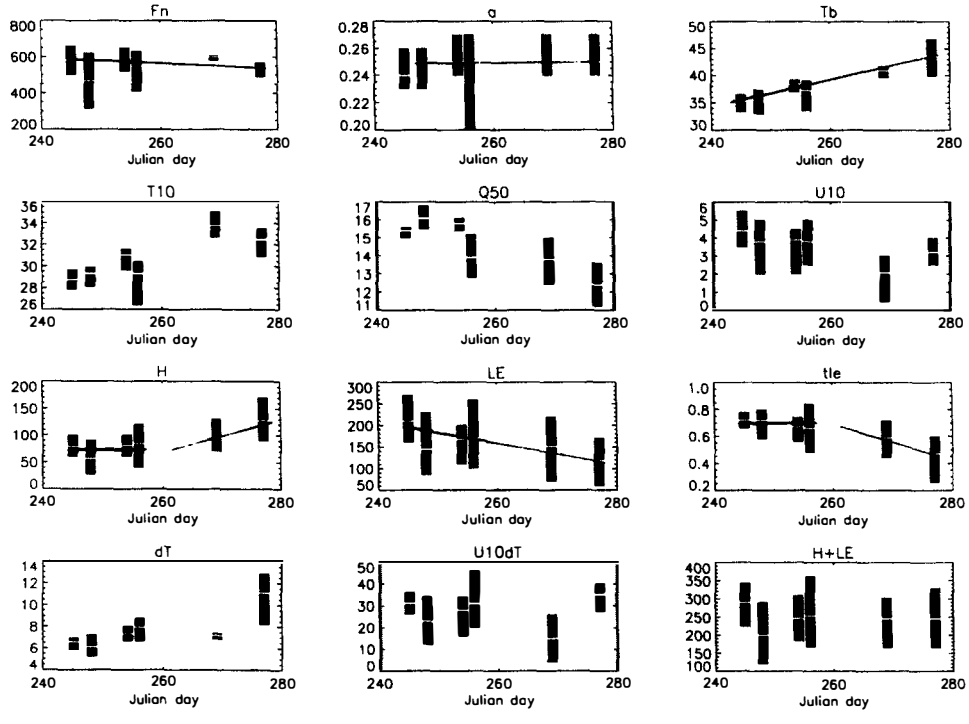

Fig. 8. Average and extreme values of the fields represented in Fig. 7.

3.3. Description of the fields

3.3.1. Flight 35 of 1/9/92

This flight was characterized by variable, but extensive, cloud cover, which produces variable net radiation. Albedo varies from 0.23 to 0.26. The field of latent heat flux shows a north–south variation from 160 to 260 W m^{-2} (109 W m^{-2} per 100 km), which is also noticeable on the humidity field (0.7 g kg^{-1} per 100 km), but has shifted to south-east for windspeed. The fields of sensible heat flux, air temperature and surface radiative temperature have a south–north gradient with values ranging from 60 to 100 W m^{-2} for flux (48 W m^{-2} per 100 km), from 27.8 to 29.6°C for air temperature (1.8°C per 100 km) and from 33.3 to 36.5°C for surface temperature (3.7°C per 100 km). The ΔT field (5.6–7.0°C) retains this meridional variation (1.9°C per 100 km), which, however, is not found in $U_{10}\Delta T$.

3.3.2. Flight 37 of 4/9/92

Among the six flights, Flight 37 is the most cloudy, as is shown by the lower, more variable net radiation (Fig. 8). The strong south–north variation (353 W m^{-2} per 100 km) of the net radiation can be related to the strong variation of the surface temperature. Albedo varies from north-east to south-west, from 0.23 to 0.26 (0.027 per 100 km). The latent heat flux field, which varies from 85 to 230 W m^{-2}, shows a south-east to north-west organization (119 W m^{-2} per 100 km), opposite to those of humidity and windspeed (15.6 to 16.6 g kg^{-1}; 0.9 g kg^{-1} 100 km for humidity). For heat transfer, there appears to be similarity between net radiation, sensible heat flux (30 to 90 W m^{-2}; 71 W m^{-2} per 100 km), air temperature at 10 m (28.1 to 29.9°C; 1.8°C per 100 km), and surface radiative temperature (32.9 to 37.3 °C; 4.7°C per 100 km). The ΔT (5.2 to 7.6 °C) and $U_{10}\Delta T$ fields are not so well organized.

3.3.3. Flight 41 of 10/9/92

Flight 41 was much sunnier than the two preceding flights, but as the surface radiative temperature was greater (35.2°C for Flight 35 and 38.4°C for Flight 41), the average net radiation is not very much greater. Albedo varies from east to west, from 0.24 to 0.27 (0.028/100 km). The latent heat flux field varies from 110 to 200 W m^{-2}. There are no organized fields for this flight, except these of albedo and air temperature (29.6 to 31.6°C; 2.6°C per 100 km). The $U_{10}\Delta T$ field, which is very different from the sensible heat flux field, seems to be mainly influenced by the wind, that is stronger than on the other days.

3.3.4. Flight 42 of 12/9/92

Flight 42 was made 2 days after Flight 41 but storms occurred between the two flights. It was previously noted that the rainfall that preceded the flight mainly affected the southern part of the flight zone, which was still saturated. One of the consequences is the variation in albedo values (0.20 to 0.27) and its organization from east to west then becoming south–north (0.04 per 100 km). The sky was again cloudy and the surface temperature increased a little; as a result the mean net radiation dropped 50 W m^{-2}. The recent rainfall also affected the variability of the other parameters such as surface temperature, air temperature, humidity and windspeed: the air mass is still unstable and the variability is

the strongest of the six flights. The latent heat flux field, like that of humidity, varies from north to south, ranging from 100 to 260 W m^{-2} (220 W m^{-2} per 100 km) and 12.8 to 15.2 g kg^{-1} (2.6 g kg^{-1} per 100 km), respectively. The sensible heat flux (40 to 120 W m^{-2}), surface radiative temperature (33.5 to 39°C, 5.6°C per 100 km) air temperature (26.4 to 30.4°C; 4.7°C per 100 km) and ΔT (6.6–8.8 °C) fields are showing a south–north gradient, with the strongest gradient in south. This different partitioning of the sensible heat flux and mean parameters between the south and the north has to be related to the spatial distribution of rainfall noted for Fig. 3 where two different areas appear: dry to the north and wet to the south. However, it is surprising that the north/south heterogeneity is not so apparent in the latent heat flux field which shows a regular north to south gradient. However, this field is consistent in the southern part with the rainfall field shown in Fig. 3 and both exhibit a maximum in the same area.

3.3.5. Flight 47 of 25/9/92

Flight 47, the first flight after the last rain, was characterized by a low cloudiness but with visibility reduced by haze. The average net radiation increased and the variations are very small. Albedo varies from east to west, from 0.24 to 0.27 (0.023 per 100 km). The latent heat flux field is represented with an accuracy of 40 W m^{-2} because of the accuracy of measurement which has decreased from 10 to 22%. As a result of this, the field produced is rather smooth. It varies from 70 to 220 W m^{-2} with a north–south organization (109 W m^{-2} per 100 km) which can also be seen in the humidity and wind fields (12.4 to 15 g kg^{-1}; 2.6 g kg^{-1} per 100 km). Sensible heat flux varies from 70 to 130 W m^{-2}. It tends to increase from south to north but the gradient is not regular (79 W m^{-2} per 100 km). The fields of air temperature at 10 m and surface radiative temperature behave similarly to that of flux (south–north gradient, a little more regular than the flux gradient, of, respectively, 2.7°C per 100 km (32.6 to 35.0°C) and 1.9°C per 100 km (39.6 to 41.8°C)). It is important to note that for this flight, the variations in ΔT (0.7°C per 100 km; 6.8 to 7.4°C) and in $U_{10}\Delta T$ are oriented north to south, the opposite to what happens with flux. It should be noted also that the values for wind at 10 m are very low for this flight, and so application of the bulk Eq. (11) is questionable.

3.3.6. Flight 53 of 3/10/92

Average net radiation for Flight 53 is less than that of the previous flight, on account of both greater cloudiness and higher surface radiative temperature. The field of albedo varies from east to west (0.031 per 100 km), from 0.24 to 0.27. The latent heat flux field, which varies from 60 to 170 W m^{-2}, presents an east–west organization of isolines (without a regular gradient) whereas wind and mixing ratio increase from north to south (2.3 g kg^{-1} per 100 km for mixing ratio which varies from 11.2 to 13.6 g kg^{-1}). The sensible heat flux field (90 to 170 W m^{-2}), with its south–north gradient of 74 W m^{-2} per 100 km, shows good similarity to those of surface radiative temperature (2.6°C per 100 km; 39.9 to 46.8°C), air temperature (2.7°C per 100 km; 30.9 to 33.5°C) and ΔT (4.8°C per 100 km; 8.5 to 13°C), but is very different from the field of $U_{10}\Delta$T which follows the wind field north–south gradient. Fig. 8 also shows a very large variability in ΔT for this flight compared with the other flights, due to the high variability in surface radiative temperature. However, this higher variability is found neither in $U_{10}\Delta T$, nor in H.

3.4. Characteristics of the different fields and temporal evolution

This section makes a synthesis of the results bringing out the characteristics common to the different flights. Fig. 8 shows the temporal variations.

The parameter which presents the same absolute value and the same spatial variability is the albedo, whose east–west gradient can be found systematically on all the flights except Flight 42, when the surface was partially saturated. This gradient should be considered in relation to the surface characteristics which were described at the beginning of this paper for the Central Supersites and the site of Danguey Gorou: thus it would seem that the reduction in vegetation from east to west (and the associated increase in surface albedo) is a general characteristic of the area under study. It is probably linked to the presence of the wetter Dallol Bosso area on its eastern perimeter. It is however surprising that the mean value of albedo remains constant during the whole month of study whereas the surface characteristics change considerably. The fact that the cloud cover was highly variable from one flight to the next could perhaps be responsible for a bias in the radiation measurements.

Another striking result is that during the whole period, marked by the end of rainfall and by the drying and warming of the air mass, the net radiation slightly decreases instead of increasing: the increase of the incoming shortwave radiation linked to the reduction in clouds is not large enough to balance the loss due to the increase in surface radiative temperature.

Some parameters present a more or less well-organized south–north gradient. They are the sensible heat flux for Flights 35, 37, 42 in the south part, 47 and 53, the surface radiative temperature and the air temperature for all flights. A corresponding gradient is found in the opposite direction (north to south) on most of the humidity fields. The gradient in air temperature and humidity is linked to the proximity of the ITCZ to the north of the area, which explains this slight variation from a warm and humid air mass to the south to a warmer and drier one to the north (in fact the monsoon layer (marine) is lying under the continental air layer but the monsoon layer becomes increasingly thinner as the ITCZ is closer). The fact that this south–north gradient is also found in the surface temperature and sensible heat flux fields reflects some variations of longer time-scales such as the climatic meridional gradient of rainfall described by Goutorbe et al. (1994). However the relationship in Eq. (11) that relates the flux to U_{10} and ΔT is hard to understand in the case of these data: the ΔT fields show most of the time (except for Flights 41 and 47) some similarity with the sensible heat flux fields, but the $U_{10}\Delta T$ spatial variation and temporal evolution are controlled by windspeed (in spite of the lower mean value of U_{10} relative to ΔT). So the organization of the $U_{10}\Delta T$ fields is very different. For instance in the case of Flight 47, this implies a major contribution of the Dalton number C_t, which is unlikely to occur. The fields of the Dalton number are not shown here because this parameter is residual in Eq. (11) and therefore involves too many inaccuracies (especially for H and ϵ). However, an attempt to check Eq. (11) by plotting $U_{10}\Delta T$ against $\overline{w't'}$ failed: C_t, the slope of the line fitted to the data, was often negative and the correlation was not significant. The low windspeed in combination with the inaccuracy of the calculation provides a plausible explanation. However the result is more encouraging if the averages of flux and mean parameters over the entire study area are used to test Eq. (11). Saïd and

Druilhet (1991) used this method with data from a neutral marine boundary layer, to show that Eq. (11) was valid from a 4-km × 4-km scale to a 50-km × 50-km one. The 'global' C_t obtained with the present results are 2.5×10^{-3}, 2.2×10^{-3}, 2.5×10^{-3}, 2.5×10^{-3}, 5.7×10^{-3} and 3.2×10^{-3} for Flights 35, 37, 41, 42, 47 and 53, respectively. The result for Flight 47 corresponds to very low wind (1.4 m s^{-1}). The other results show that a Stanton number at the scale of 90 km × 75 km, shows a trend to increase as the conditions dry. However, this would need further investigation and confirmation from other flights.

For latent heat flux, the north–south gradient, as might be expected from the humidity and windspeed north–south gradient, is not encountered systematically. However, the surface moisture is not available and is lacking in the interpretation, though it must make a major contribution. The only thing that can be said from Fig. 8 is that the range of variability of *LE* remains roughly constant during the whole period so the relative variability (absolute variability/flux value) increases as the flux decreases. Moreover, the lengthscales of the variability decrease: this is not apparent on the fields which were smoothed to keep enough significance, but has been proved by the study on the integral scales and correlation coefficients in Section 3.1.

Heterogeneity in the latent heat flux occurred on Flight 42, after storms that affected the south part of the area only. From this day, the surface dried out and its moisture became highly variable according to the amount and frequency of rainfall it had received but also according to the soils' capacity to store the water or let it run off or infiltrate. However, the surface is probably not entirely responsible for the observed heterogeneity: the low frequency scales that are encountered at the end of the period are the evidence that this heterogeneity affects the whole boundary layer depth and should be related to the fact that the monsoon layer becomes thinner. Taylor et al. (1997) study the situation of 8 October (5 days after Flight 53) and they point out the influence of the continental layer, to the north of the study area.

4. Conclusion

Measurements of sensible and latent heat fluxes, radiative fluxes, windspeed, air temperature and humidity, collected by the Météo France Merlin IV aircraft are presented here for six meteorological conditions during the HAPEX-Sahel experiment: four during the rainy season, and two at the beginning of the dry season.

A study of the flux estimation accuracy led to a study of the sample length along which fluxes are calculated (by the eddy correlation method). This study revealed that the behaviour of the latent heat flux is highly variable, depending on the hydrological conditions: the latent heat transfers are very heterogeneous at the beginning of the dry season whereas they behave like the sensible heat transfers during the rainy season. The consequence is that the minimum length which can be used to compute turbulent fluxes is, for an accuracy of 20%:

- 7 km for sensible heat flux under wet or dry conditions
- 10 km for latent heat under wet conditions
- 30 km for latent heat under dry conditions

These lengths can be considered as the minimum length scale at which aircraft fluxes can be computed for modelling comparisons.

In this study, the objective is to try to find repetitive features in the transfers and the apparent driving parameters so that the flux spatial variability can be understood, and perhaps forecast. To do that, bidimensional fields of the parameters that were measured over a 90-km × 75-km area were constructed. The fields were constructed using samples 25 km long in order to obtain an accuracy that remained smaller than the spatial variability (the accuracy is then about 12%, except for the latent heat flux under dry conditions for which the accuracy is 23%). The obtained fields were well organized and showed in several cases, regular and repetitive gradients. The most important results are:

- Although the sky clears with the end of the rainy season, the available energy does not increase, due to the increase of the surface radiative temperature.
- The albedo shows an east–west gradient, which indicates a variation of the surface conditions due to the closeness of the Dallol Bosso valley, to the east of the studied area.
- The sensible heat flux presents in several cases a south–north gradient that can be related to the climatic meridional gradient characteristic of the Sahelian area. This gradient is systematically found in the surface radiative temperature fields and often in the air temperature but less often in the ΔT fields. This means that ΔT is not the only parameter to drive the sensible heat flux. However, the windspeed at 10 m is not a pertinent parameter to drive the flux in the conditions studied here, because it is most of the time rather low and its gradient never oriented in the same direction as the flux gradient. The study could not be extended any longer due to the lack of accuracy of the Stanton number. However, if the bulk formula is applied at the scale of the whole study area and if we reject the case when the wind was too low, we obtain Stanton numbers slightly increasing from 2.2 to 3.2×10^{-3} during the period, which is encouraging for modelling purposes at this scale.
- The latent heat flux as well as the humidity and the windspeed less often contain any north–south gradient. However, for lack of surface humidity information it was not possible to derive a quantitative relationship between the flux and the surface water content.
- The most important result of this study is the different spectral behaviour of the two heat fluxes. This first implies that in some cases, the similarity relationships used for the surface or mixed layer, should make a difference between t and q. The second conclusion is that the latent heat flux (and probably also the sensible heat flux) are not only directed by local turbulence but by atmospheric organizations at the boundary layer scale. So it would be illusive, for remote-sensing purposes, to try to predict any surface flux value, without a sophisticated 3D model.

Acknowledgements

We should like to express our gratitude towards those in charge of the HAPEX Sahel campaign, M. Hoepffner, J.P. Goutorbe and T. Lebel who helped set up and organize the

operation. We should also like to thank the engineers and technicians of Météo France who fitted out the planes, performed the flights and supplied the measurements presented above. We are also grateful to A. Herrada, for taking care of administrative and accounting tasks to enable our participation, as well as to the computer experts in our laboratory. We are indebted to T. Lebel, J.D. Taupin and their research team at ORSTOM who provided to the HAPEX Sahel data base the rainfall data we used here. We also thank J. Gash and his co-authors in Gash et al. (1997) for the use of their figure on evaporative fraction for comparison with aircraft measurements. We would like to thank gratefully S. Prince for his advice and encouragement. Thanks also to the team who implemented the data base and who goes on managing it. Constructive criticism by reviewers has also been much appreciated. The Centre National d'Etudes Spatiales provided the support for the data base. Our operation was supported by the Institut National des Sciences de l'Univers.

References

André, J.C., Goutorbe, J.P., Perrier, A., Becker, F., Bessemoulin, P., Bougeault, P., Brunet, Y., Brutsaert, W., Carlson, T., Cuenca, R., Gash, J., Gelpe, J., Hildebrand, P., Lagouarde, J.P., Lloyd, C., Mahrt, L., Mascart, P., Mazaudier, C., Noilhan, J., Ottlé, C., Payen, M., Phulpin, T., Stull, R., Shuttleworth, J., Schmugge, T., Taconet, O., Tarrieu, C., Thepenier, R.M., Valencogne, C., Vidal-Madjar, D. and Weill, A., 1988. Evaporation over land-surface: first results from HAPEX-MOBILHY special observing period. Ann. Geophys., 6(5): 477–492.

André, J.C., Bougeault, P. and Goutorbe, J.P.G., 1990. Regional estimates of heat and evaporation fluxes over non-homogeneous terrain. Examples from the HAPEX-MOBILHY programme. Bound. Lay. Met., 50: 77–108.

Betts, A.K., Desjardins, R.L. and Macpherson, J.I., 1992. Budget analysis of the boundary layer grid flights during FIFE 1987. J. Geophys. Res., 97(D17): 18533–18546.

Bolle, H.J., André, J.C., Arrue, J.L., Barth, H.K., Bessemoulin, P., Brasa, A., de Bruin, H.A.R., Cruces, J., Dugdale, G., Engman, E.T., Evans, D.L., Fantechi, R., Fiedler, F., van de Griend, A., Imeson, A.C., Jochum, A., Kabat, P., Kratzsch, T., Lagouarde, J.P., Langer, I., Llamas, R., Lopez-Baeza, E., Melia Miralles, J., Muniosguren, L.S., Nerry, F., Noilhan, J., Oliver, H.R., Roth, R., Saatchi, S.S., Sanchez Diaz, J., de Santa Olalla, M., Shuttleworth, W.J., Sogaard, H., Stricker, H., Thornes, J., Vauclin, M. and Wickland, D., 1993. EFEDA: European Field Experiment in a Desertification-threatened area. Ann. Geophys., 11: 173–189.

Brown, E.N., Friehe, C.A. and Lenschow, D.H., 1983. The use of pressure fluctuations on the nose of an aircraft for measuring air motion. J. Clim. Appl. Meteorol., 22: 171–180.

Brutsaert, W. and Sugita, M., 1992. Application of self-preservation in the diurnal evolution of the surface energy budget to determine daily evaporation. J. Geophys. Res., 97(D17): 18377–18382.

Davis, F.W., Schimel, D.S., Friedl, M.A., Michaelsen, J.C., Kittel, T.G.F., Dubayah, R. and Dozier, J., 1992. Covariance of biophysical data with digital topographic and land use maps over the FIFE site. J. Geophys. Res., 97(D17): 19009–19022.

Desjardins, R.L., Schuepp, P.H., MacPherson, J.I. and Buckley, D.J., 1992. Spatial and temporal variations of the fluxes of carbon dioxide and sensible and latent heat over the FIFE site. J. Geophys. Res., 97(D17): 18467–18475.

d'Herbès, J.M. and Valentin, C., 1997. Land surface conditions of the Niamey region: ecological and hydrological implications. J. Hydrol, this issue.

Druilhet, A., Frangi, J.P., Guédalia, D. and Fontan, J., 1983. Experimental studies of the turbulence structure parameters of the convective boundary layer. J. Clim. Appl. Met., 22(4): 594–608.

Durand, P., 1983. Etude des caractéristiques turbulentes de la couche limite convective sahélienne (expérience ECLATS). Thèse de docteur-ingénieur, No. 826, Université Paul Sabatier, Toulouse, France.

Dyer, A.J. and Hicks, B.B., 1970. Flux-gradient relationships in the constant flux layer. Q.J.R. Met. Soc., 96: 715–721.

Estèves, M., 1994. Cartographie d'unités hydrologiques homogènes et modélisation hydrologique, exemple de l'expérience HAPEX Sahel. Actes des Xèmes Journées hydrologiques, ORSTOM.

Estèves, M. and Lenoir, F., 1994. Un exemple de fonctionnement hydrologique dans le bassin de Sama Dey. Actes des Xèmes Journées hydrologiques, ORSTOM.

Gash, J.H.C., Kabat, P., Amadou, M., Bessemoulin, P., Billing, H., Blyth, E.M., deBruin, H.A.R., Elbers, J.A., Friborg, T., Harrison, G., Holwill, C.J., Lloyd, C.R., Lhomme, J.P., Moncrieff, J.B., Monteny, B.A., Puech, D., Sögaard, H., Tuzet, A. and Verhoef, A., 1997. The variability of evaporation during the HAPEX-Sahel intensive observation period. J. Hydrol., this issue.

Goutorbe, J.P., Lebel, T., Tinga, A., Brouwer, J., Dolman, A.J., Engman, E.T., Gash, J.H.C., Hoepffner, M., Kabat, P., Monteny, B., Prince, S., Saïd, F., Sellers, P. and Wallace, J., 1994. HAPEX Sahel: a large scale study of land–atmosphere interactions in the semi-arid tropics. Ann. Geophysicae, 12: 53–64.

Grossman, R.L., 1992. Sampling errors in the vertical fluxes of potential temperature and moisture measured by aircraft during FIFE. J. Geophys. Res., 97(D17): 18439–18444.

Hildebrand, P.H., 1991. Errors in eddy correlation turbulence measurements from aircraft: application to HAPEX-MOBILHY. In: T.J. Schmugge and J.C. André (Editors), Land Surface Evaporation. Springer-Verlag.

Lebel, T., Sauvageot, H., Hoepffner, M., Desbois, M., Guillot, B. and Hubert, P., 1992. Rainfall estimation in the Sahel: the EPSAT-Niger experiment. Hydrolog. Sci., 37(3): 6.

Lenschow, D.H. and Stankov, B.B., 1986. Length scales in the convective boundary layer. J. Atmos. Sci., 43: 1198–1209.

Lenschow, D.H., Wyngaard, J.C. and Pennell, W.T., 1980. Mean-field and second-moment budgets in a baroclinic, convective boundary layer. J. Atmos. Sci., 37: 1313–1326.

Lenschow, D.H., Mann, J. and Kristensen, L., 1994. How long is long enough when measuring fluxes and other turbulence statistics? J. Atm. Ocean. Tec., 11: 661–673.

Lloyd, C.R., Bessemoulin, P., Cropley, F.D., Culf, A.D., Dolman, A.J., Elbers, J., Heusinkveld, B., Moncrieff, J.B., Monteny, B. and Verhoef, A., 1997. A comparison of surface fluxes at the HAPEX-Sahel bush sights. J. Hydrol., this issue.

Lumley, J.L. and Panofsky, H.A., 1964. The Structure of Atmospheric Turbulence. Interscience, 239 pp.

Mahrt, L., 1987. Grid-averaged surface fluxes. Mon. Weather Rev., 115: 1550–1560.

Mahrt, L., 1991. Boundary-layer moisture regimes. Q.J.R. Meteorol. Soc., 117: 151–176.

Mahrt, L., Macpherson, J.I. and Desjardins, R., 1994. Observations of fluxes over heterogeneous surfaces. Bound. Lay. Met., 67: 345–364.

Mann, J. and Lenschow, D.H., 1994. Errors in airborne flux measurements. J. Geophys. Res., 99(D7): 14519–14526.

Mason, P.J., 1988. The formation of aereally-averaged roughness lengths. Q.J.R. Met. Soc., 114: 399–420.

Moeng, C.H. and Wyngaard, J.C., 1989. Evaluation of turbulent transport and dissipation closures in second-order modeling. J. Atmos. Sci., 46: 2311–2330.

Peugeot, C., Cappelaere, B., Chevallier, P., Estèves, M., Galle, S., Rajot, J.L. and Vandervaere, J.P., 1994. Mod élisation hydrologique sur le supersite central est d'HAPEX Sahel. Première étape: des parcelles exp érimentales aux micro-bassins versants. Actes des Xèmes Journées hydrologiques, l'ORSTOM.

Peugeot, C., Esteves, M., Rajot, J.L., Vandervaere, J.P. and Galle, S., 1997. Run-off generation processes: results and analysis of field data collected at the East Central Supersite of the HAPEX-Sahel experiment. J. Hydrol., this issue.

Prince, S.D., Kerr, Y.H., Goutorbe, J.P., Lebel, T., Tinga, A., Brouwer, J., Dolman, A.J., Engman, E.M., Kabat, P., Monteny, B., Saïd, F., Sellers, P. and Wallace, J., 1995. Geographical, biological and remote sensing aspects of the Hydrologic Atmospheric Pilot Experiment in the Sahel (HAPEX-Sahel). Remote Sens. Environ., 51(1): 215–234.

Saïd, F. and Druilhet, A., 1991. Experimental study of the marine boundary layer from in-situ aircraft measurements (TOSCANE-T campaign): variability of boundary conditions and eddy flux parameterization. Bound. Lay. Met., 57: 219–249.

Schmugge, T.J. and André, J.C., 1991. Land Surface Evaporation. Measurement and Parameterization. Springer-Verlag.

Segal, M., Garratt, J.R., Kallos, G. and Pielke, R.A., 1988. The impact of wet soil and canopy temperatures on daytime boundary-layer growth. J. Atmos. Sci., 46: 3673–3684.

Segal, M., Schreiber, W.B., Kallos, G., Garratt, J.R., Roding, A., Weaver, J. and Pielke, R.A., 1989. The impact of crop areas in northeast Colorado on midsummer mesoscale thermal circulations. Mon. Weather Rev., 117: 809–825.

Sellers, P.J., Hall, F.G., Asrar, G., Strebel, D.E. and Murphy, R.R., 1988. The first ISLSCP field experiment (FIFE). Bull. Am. Meteorol. Soc., 69: 22–27.

Sellers, P.J., Hall, F.G., Asrar, G., Strebel, D.E. and Murphy, R.E., 1992. An overview of the first International Satellite Land Surface Climatology Project (ISLSCP) Field Experiment (FIFE). J. Geophys. Res., 97(D17): 345–371.

Taylor, C.M., Harding, R.J., Thorpe, A.J. and Bessemoulin, P., 1997. A mesoscale simulation of land surface heterogeneity from HAPEX-Sahel. J. Hydrol., this issue.

Wai, M.M.K., Smith, E.A., Bessemoulin, P., Culf, A.D., Dolman, A.J. and Lebel, T., 1997. Variability in boundary layer structure during HAPEX-Sahel: wet–dry season transition. J. Hydrol., this issue.

Wyngaard, J.C., 1973. On surface-layer turbulence. In: D.A. Haugen (Editor), Workshop on Micrometeorology. Am. Meteorol. Soc., pp. 101–149.

Wyngaard, J.C., 1982. Boundary layer modeling. In: F.T.M. Niewstadt and H. van Dop (Editors), Atmospheric Turbulence and Air Pollution Modelling. Reidel, pp. 69–106.

Wyngaard, J.C., 1983. Lectures on planetary boundary-layer. In: D. Lilly and T. Galchen (Editors), Mesoscale Meteorology – Theory, Observations and Models. Reidel, Hingham, MA, pp. 603–650.

Wyngaard, J.C., Coté, O.R. and Izumi, Y., 1971. Local free convection, similarity and the budgets of shear stress and heat flux. J. Atmos. Sci., 28: 1171–1182.